



Schwinger boson symmetric spin liquids of Shastry-Sutherland model

Ke Liu *International Center for Quantum Materials, School of Physics, Peking University, Beijing 100871, China*Fa Wang **International Center for Quantum Materials, School of Physics, Peking University, Beijing 100871, China
and Collaborative Innovation Center of Quantum Matter, Beijing 100871, China* (Received 8 September 2023; revised 10 January 2024; accepted 18 March 2024; published 5 April 2024)

Motivated by recent experimental and numerical evidence of deconfined quantum critical points and quantum spin liquid states in the spin-1/2 Heisenberg model on the Shastry-Sutherland lattice, we studied possible symmetric spin liquid states and their proximate ordered states under Schwinger boson formalism. We found a symmetric gapped Z_2 spin liquid state for intermediate model parameter $0.66 < J_1/J_2 < 0.71$ under the mean-field approximation. The Schwinger boson mean-field picture is partially supported by exact-diagonalization and self-consistent spin wave theory results.

DOI: [10.1103/PhysRevB.109.134409](https://doi.org/10.1103/PhysRevB.109.134409)

I. INTRODUCTION

Recently the quasi-two-dimensional materials $S = 1/2$ quantum magnets $\text{SrCu}_2(\text{BO}_3)_2$ [1–4] have attracted much research interest, as they are one of the most promising realizations of the deconfined quantum critical point (DQCP) [5–8] or spin liquid states [9]. The in-plane antiferromagnetic (AFM) Heisenberg interactions between the copper atoms of $\text{SrCu}_2(\text{BO}_3)_2$ make it a potential realization of the Shastry-Sutherland model [10] shown in Fig. 1(a). Depending on the values of the nearest-neighbor couplings J_1 and the second-neighbor couplings J_2 , the Shastry-Sutherland model can host a dimer valence bond solid ground state in the $J_2/J_1 \gg 1$ limit, or a Néel state in the $J_1/J_2 \gg 1$ limit. The issue is the intermediate phase [11–14] between the Néel phase and dimer-singlet (DS) phase [also called the orthogonal dimer (OD) phase in some literature]. There is a variety of predictions of the intermediate phase by difference theories and numerics: a direct transition from the dimer-singlet phase to Néel phase [15,16], a helical order [17,18], columnar dimers [19], or plaquette-singlet [12,16,18] intermediate phases. Recently there has been experimental [2–4] and numerical [14,20–23] evidence of the existence of the plaquette-singlet (PS) phase [also called the plaquette singlet solid (PSS) or plaquette valence bond solid (PVBS) in some literature]. The phase transition between the Néel and plaquette-singlet phase may be described by a DQCP with emergent $O(4)$ symmetry [13,20] and deconfined spinon excitations. And evidence of a proximate DQCP was found on the boundary of plaquette-singlet phase and Néel AFM phase in an NMR study of $\text{SrCu}_2(\text{BO}_3)_2$ under external magnetic field [1].

Some recent numerical studies including density-matrix renormalization group (DMRG) [24], exact diagonalization

(ED) [25], and pseudofermion functional renormalization group [26] also suggest the existence of a spin liquid (SL) phase in a narrow range of coupling parameter J_1/J_2 between the PS phase and Néel phase without magnetic field. This intriguing possibility has not been thoroughly studied theoretically, especially using the traditional slave particle language for spin liquids [27]. With this motivation we study the possible symmetric spin liquid states and their proximate ordered states on the Shastry-Sutherland lattice under the Schwinger boson formalism [28] in this paper. The goal of our work is not to accurately determine the phase diagram of the Shastry-Sutherland model, but to explore the possibilities of quantum spin liquids compatible with this lattice, which might be realized in related models and materials.

In this paper, we focus on the Schwinger boson [29] description of quantum spin liquids. This formalism and its large- N generalization [30] are convenient to describe the transition between gapped Z_2 spin liquid phases and magnetic ordered phases [28], and have been successful in studies of several quantum magnets [31]. By projective symmetry group (PSG) [32,33], we find 6 possible algebraic Z_2 PSG solutions and 4 gauge-inequivalent *Ansätze*. Comparing the mean-field energies of these *Ansätze*, we get the mean-field phase diagram, which is shown in Fig. 1. We find a symmetric gapped Z_2 spin liquid for the intermediate model parameter $0.66 < J_1/J_2 < 0.71$ under the mean-field approximation. A dimer-singlet phase forms in $J_1/J_2 < 0.66$ while a Néel AFM state forms in $J_1/J_2 > 0.71$, where the Schwinger boson condensation happens. To further investigate the PS state, we also study *Ansätze* with PS order, and find that these PS *Ansätze* have higher ground state energy compared with the symmetric spin liquids in the mean-field level.

We also study the spin correlations of the ground state wave function and structure factor of the spin liquid states and Néel state by the Schwinger boson mean-field theory (SBMFT), and compare them with the results of exact-diagonalization

*wangfa@pku.edu.cn

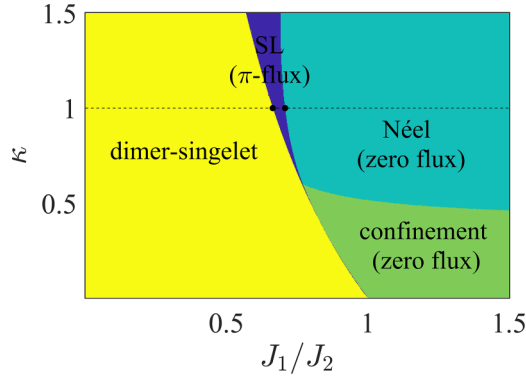


FIG. 1. The phase diagram of Schwinger boson mean-field theory for Shastry-Sutherland model. The phase boundaries at physical condition $\kappa = 2S = 1$ are $J_1/J_2 = 0.66$ and $J_1/J_2 = 0.71$. In the mean-field level, the phase transition from DS to SL is continuous while the phase transition from SL to Néel is first order.

and spin wave theory. We find that the spin correlations in SBMFT have similar behavior compared with the result of the exact-diagonalization method. The structure factor in the Néel phase can also be calculated by the spin wave theory. However, the linear spin wave theory breaks down near $J_1/J_2 \sim 1$, which is far from the Néel phase boundary. To investigate the Néel phase in the $J_1/J_2 < 1$ region, we use a self-consistent spin wave theory, which pushes the Néel phase boundary down to $J_1/J_2 \approx 0.65$. With the self-consistent spin wave theory, we get qualitatively consistent dynamical spin correlations with Schwinger boson mean-field theory.

This paper is organized as follows. In Sec. II, we introduce the Shastry-Sutherland model and Schwinger boson mean-field theory. We then introduce the PSG classification and show the results of algebraic PSG. In Sec. III, we show the mean-field results and properties of the 4 gauge-inequivalent symmetric spin liquid states, and briefly discuss the two PS states. In Sec. IV, we present the mean-field phase diagram with a gapped Z_2 spin liquid state in the intermediate parameter $0.66 < J_1/J_2 < 0.71$. In Sec. V, we compare the structure factors for the spin liquid and Néel states by SBMFT and self-consistent spin wave theory, and compare some of the ground state properties by SBMFT and exact diagonalization. Section VI contains further discussion and a summary of results. The technical and numerical details are presented in the appendices.

II. PROJECTIVE SYMMETRY GROUP OF SHASTRY-SUTHERLAND LATTICE SCHWINGER BOSON STATES

The Shastry-Sutherland model Hamiltonian is

$$H = J_1 \sum_{\langle ij \rangle} \mathbf{S}_i \cdot \mathbf{S}_j + J_2 \sum_{\langle\langle ij \rangle\rangle'} \mathbf{S}_i \cdot \mathbf{S}_j, \quad (1)$$

where \mathbf{S}_i are $S = 1/2$ spin operators and $\langle ij \rangle$ are the nearest-neighbor (n.n.) [blue in Fig. 2(a)] bonds, while $\langle\langle ij \rangle\rangle'$ are some of the next-nearest-neighbor (n.n.n.) [red in Fig. 2(a)]

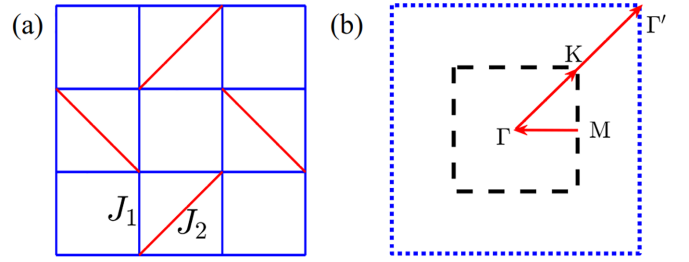


FIG. 2. (a) is the Shastry-Sutherland lattice. The Heisenberg couplings in blue and red bonds are J_1 and J_2 , respectively. The black dashed line in (b) is the first Brillouin zone of Shastry-Sutherland lattice, and the blue dotted line is the first Brillouin zone of square lattice without J_2 bonds. The red arrows are the plot paths ($K \rightarrow M \rightarrow \Gamma \rightarrow K \rightarrow \Gamma'$) in this paper.

bonds. Here we study this Hamiltonian by the Schwinger boson mean-field theory. The spin operator is expressed by the Schwinger bosons as

$$\mathbf{S}_i = \frac{1}{2} \sum_{\alpha, \beta = \uparrow, \downarrow} b_{i\alpha}^\dagger \boldsymbol{\sigma}_{\alpha\beta} b_{i\beta}, \quad (2)$$

with the constraints at every site

$$\sum_{\sigma} b_{i\sigma}^\dagger b_{i\sigma} = \kappa = 2S, \quad (3)$$

for a spin system with spin S . For the convenience of analysis, κ is usually regarded as a continuous parameter. Using the Schwinger boson representation, the Heisenberg interaction can be rewritten as

$$\mathbf{S}_i \cdot \mathbf{S}_j =: \hat{B}_{ij}^\dagger \hat{B}_{ij} : - \hat{A}_{ij}^\dagger \hat{A}_{ij}, \quad (4)$$

where $::$ is normal ordering and boson pairing operator \hat{A} and hopping operator \hat{B} are defined as

$$\hat{B}_{ij} = \frac{1}{2} \sum_{\sigma} b_{i\sigma}^\dagger b_{j\sigma}, \quad (5)$$

$$\hat{A}_{ij} = \frac{1}{2} \sum_{\sigma, \sigma'} \epsilon_{\sigma\sigma'} b_{i\sigma} b_{j\sigma'}. \quad (6)$$

After decoupling the quartic terms by the Hubbard-Stratonovich transformation, we get the mean-field Hamiltonian:

$$H_{\text{MF}} = \sum_{ij} J_{ij} (-A_{ij}^* \hat{A}_{ij} + B_{ij}^* \hat{B}_{ij} + \text{H.c.}) + \sum_{ij} J_{ij} (|A_{ij}|^2 - |B_{ij}|^2) - \mu_i \sum_i (\hat{n}_i - \kappa), \quad (7)$$

where the complex numbers $A_{ij} = \langle \hat{A}_{ij} \rangle = -A_{ji}$ and $B_{ij} = \langle \hat{B}_{ij} \rangle = B_{ji}^*$ are the mean-field *Ansätze*. μ_i are the real Lagrangian multipliers to enforce the constraints of Eq. (3), which are usually site independent, namely $\mu_i = \mu$. This mean-field description has emergent $U(1)$ gauge redundancy,

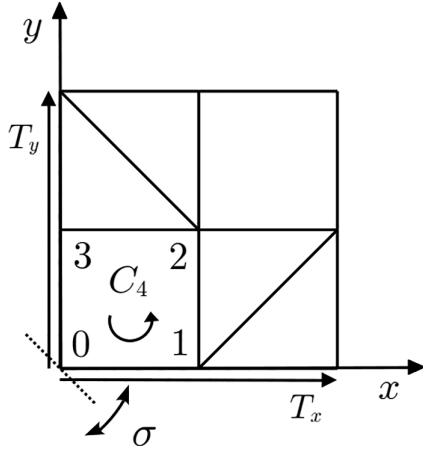


FIG. 3. The coordinate system and space group generators T_x , T_y , C_4 , σ of the Shastry-Sutherland lattice. These generators are translation T_x along \hat{e}_x by 2 units, translation T_y along \hat{e}_y by 2 units, a reflection σ about $x = -y$ and the 90° rotation C_4 around $(1/2, 1/2)$.

namely that the following $U(1)$ gauge transformation,

$$b_{j\sigma} \rightarrow e^{i\phi(j)} b_{j\sigma}, \quad (8a)$$

$$A_{ij} \rightarrow e^{i[\phi(i)+\phi(j)]} A_{ij}, \quad (8b)$$

$$B_{ij} \rightarrow e^{i[-\phi(i)+\phi(j)]} B_{ij}, \quad (8c)$$

will not change the physical spin states. Therefore the mean-field solutions should be classified by projective symmetry group (PSG) [32,33]. In the remainder of this section, we briefly show the details of PSG classification of the symmetric spin liquid on the Shastry-Sutherland lattice.

As mentioned above, the Schwinger boson mean-field theory has an emergent $U(1)$ gauge symmetry. After the local gauge transformation of Eq. (8), the mean-field Hamiltonian is invariant and all physical observables are unchanged, as the wave function is the same after projected to physical condition. Because of the existence of emergent gauge symmetry, for different spin liquids with the same symmetry, the *Ansätze* are invariant under symmetry transformations followed by gauge transformations, $\hat{b}_{r,s} \rightarrow \exp[i\phi_g(gr)]\hat{b}_{gr,s}$, for space group element g . Therefore, the spin liquid states should be classified by the projective representation of the space group. The *Ansätze* are invariant under operations of projective symmetry group (PSG). Different PSGs characterize different kinds of spin liquid states with the same symmetries.

We set up a Cartesian coordinate system and represent the site coordinate by $(x, y) = x\hat{e}_x + y\hat{e}_y$ with $x, y \in \mathbb{Z}$. For the convenience of discussion, the site coordinate can also be expressed by cell-sublattice index, (X, Y, s) , where $X, Y \in \mathbb{Z}$ and $s \in \mathbb{Z}_4$ ($s = 0, 1, 2, 3$), which means Cartesian $(2X + x_s, 2Y + y_s)$ with $(x_0, y_0) = (0, 0)$, $(x_1, y_1) = (1, 0)$, $(x_2, y_2) = (1, 1)$, $(x_3, y_3) = (0, 1)$. The sublattice labeling is shown in Fig. 3. With these two coordinate systems, the nearest-neighbor (n.n.) bonds are $(x, y) - (x + 1, y)$ and $(x, y) - (x, y + 1)$ while the next-nearest-neighbor (n.n.n.) bonds are $(X, Y, 0) - (X, Y - 1, 2)$ and $(X, Y, 1) - (X + 1, Y, 3)$.

The space group of the square lattice is generated by translation T_x along \hat{e}_x by 2 units, translation T_y along \hat{e}_y by 2 units,

a reflection σ along $x = -y$, and the 90° rotation C_4 around $(1/2, 1/2)$, which are also shown in Fig. 3. The action of these generators on the Shastry-Sutherland lattice reads

$$T_X : (x, y) \mapsto (x + 2, y), \quad (9a)$$

$$T_Y : (x, y) \mapsto (x, y + 2), \quad (9b)$$

$$C_4 : (x, y) \mapsto (-y + 1, x), \quad (9c)$$

$$\sigma : (x, y) \mapsto (-y, -x). \quad (9d)$$

Note that the glide-reflection generators (G_x and G_y) can be generated by these four generators, which can be written as

$$G_x = C_4\sigma : (x, y) \mapsto (x + 1, -y), \quad (10)$$

$$G_y = T_y\sigma C_4 : (x, y) \mapsto (-x, y + 1), \quad (11)$$

and are not used in solving PSGs.

These 4 generators in Eq. (9) have the following commutative relations,

$$T_X^{-1}T_Y T_X T_Y^{-1} = \mathbb{1}, \quad (12)$$

$$T_Y^{-1}T_X^{-1}C_4 T_X C_4^{-1} = \mathbb{1}, \quad (13)$$

$$T_X^{-1}C_4 T_Y^{-1}C_4^{-1} = \mathbb{1}, \quad (14)$$

$$C_4^4 = \mathbb{1}, \quad (15)$$

$$T_X^{-1}\sigma T_Y^{-1}\sigma^{-1} = \mathbb{1}, \quad (16)$$

$$T_Y^{-1}\sigma T_X^{-1}\sigma^{-1} = \mathbb{1}, \quad (17)$$

$$\sigma^2 = \mathbb{1}, \quad (18)$$

$$T_X^{-1}C_4\sigma C_4\sigma^{-1} = \mathbb{1}. \quad (19)$$

We have solved the algebraic PSG in Appendix A and we only show the results here,

$$\phi_{T_X}(X, Y, s) = 0, \quad (20)$$

$$\phi_{T_Y}(X, Y, s) = 0, \quad (21)$$

$$\phi_{C_4}(X, Y, s) = p_2\pi \cdot Y + p_4\pi \cdot \delta_{s,0}, \quad (22)$$

$$\phi_\sigma(X, Y, s) = \frac{p_7\pi}{2} + p_2\pi \cdot x_s y_s + p_4\pi \cdot \delta_{s,0}, \quad (23)$$

with three remaining free \mathbb{Z}_2 integer parameters $p_2, p_4, p_7 = 0$ or 1 (mod 2). Therefore, there are at most 8 kinds of PSGs.

Then we need to consider the constraints on PSG by *Ansätze*. The n.n. bond poses no constraint, because there is no nontrivial space group element that maps one n.n. bond to itself or its reverse. For the n.n.n. bond, if $A_{n.n.n.} \neq 0$, consider $(0, 0, 0) - (0, -1, 2)$, which is invariant under σ ; then $\phi_\sigma(0, 0, 0) + \phi_\sigma(0, -1, 2) = p_7\pi + p_2\pi + p_4\pi = 0$, namely $p_2 + p_4 + p_7 = 0$; if $B_{n.n.n.} \neq 0$, consider $(0, 0, 0) - (0, -1, 2)$, which is invariant under σ ; then $\phi_\sigma(0, 0, 0) - \phi_\sigma(0, -1, 2) = -p_2\pi - p_4\pi = 0$, namely $p_2 + p_4 = 0$; this is incompatible with $A_{n.n.n.} \neq 0$; consider $(-1, 0, 1) - (0, 0, 3)$, which is reverted by σ ; then $\phi_\sigma(-1, 0, 1) - \phi_\sigma(0, 0, 3) = 0$; then if $B_{n.n.n.} \neq 0$, it must be real. If we only consider the condition where at least one of next-nearest-neighbor *Ansätze* $A_{n.n.n.}$ and $B_{n.n.n.}$ is not zero, there are at most 6 kinds of PSGs with these constraints. If we assume the nearest-neighbor *Ansatz* A_1 is nonzero, these

6 states can be classified by two gauge-invariant phases Φ_1 and Φ_2 , which are defined on empty-square plaquettes and J_2 -square plaquettes, respectively,

$$A_{ij}(-A_{jk}^*)A_{kl}(-A_{li}^*) = |A_1|^4 e^{i\Phi}. \quad (24)$$

The gauge-invariant ‘‘flux’’ values Φ_1 and Φ_2 in the empty squares and J_2 squares, respectively, are defined as the complex phase of the product of nearest-neighbor boson pairing *Ansätze* $A_{ij}(-A_{jk}^*)A_{kl}(-A_{li}^*)$ around a plaquette [34]. Due to time-reversal symmetry, Φ_1 and Φ_2 can only be 0 or π , and the four different combinations of (Φ_1, Φ_2) correspond to the 4 gauge-inequivalent *Ansätze* solved by PSG. Therefore, the 6 PSG states only have 4 gauge-inequivalent *Ansätze* which are named as (π, π) -, $(0, \pi)$ -, $(\pi, 0)$ -, and $(0,0)$ -flux states according to their gauge flux distribution. The configuration details of these states are shown in Appendix A.

III. MEAN-FIELD STATES

In this section we will show the properties of these four gauge-inequivalent spin liquid states, including the *Ansatz* amplitudes, spinon dispersions, and the static and dynamic spin structure factors.

In the Schwinger boson mean-field theory, the structure factor can be expressed by the imaginary part of ‘‘bubble’’ Feynman diagrams. Note that the anomalous Green’s function of the spinons also takes important parts. The static and dynamic spin structure factor can be measured experimentally by neutron scattering. In the following we will show the mean-field results of the four gauge-inequivalent symmetric spin liquid states. To consider the existence of the PS phase, we also briefly discuss the PS states in the open square and J_2 square, which are not included in the symmetric spin liquid states because they break the glide symmetry generated by G_x and G_y .

All these mean-field *Ansätze* have the four-site unit cell depicted in Fig. 3 and the *Ansatz* configurations are shown in the figures in Appendix A. After Fourier transformation $b_{\mathbf{s}\mathbf{k}} = \frac{1}{\sqrt{N_c}} \sum_{\mathbf{r}} e^{-i\mathbf{k}\cdot\mathbf{r}} b_{\mathbf{r}\mathbf{s}}$, where $\mathbf{r} = (X, Y)$ labels the unit cell and N_c is the number of unit cells, the mean-field Hamiltonian in Eq. (7) can be formally written as

$$H_{\text{MF}} = \sum_{\mathbf{k}} \Psi_{\mathbf{k}}^\dagger D_{\mathbf{k}} \Psi_{\mathbf{k}} + N_c [\mu + \mu\kappa + 8J_1(|A_1|^2 - |B_1|^2) + 2J_2(|A_2|^2 - |B_2|^2)], \quad (25)$$

where we have used the Nambu spinor $\Psi_{\mathbf{k}} = (b_{0\mathbf{k}\uparrow}, b_{1\mathbf{k}\uparrow}, b_{2\mathbf{k}\uparrow}, b_{3\mathbf{k}\uparrow}, b_{0-\mathbf{k}\downarrow}^\dagger, b_{1-\mathbf{k}\downarrow}^\dagger, b_{2-\mathbf{k}\downarrow}^\dagger, b_{3-\mathbf{k}\downarrow}^\dagger)^T$. A_1 and B_1 are boson pairing and hopping *Ansatz* amplitudes on n.n. bonds, respectively, and A_2 and B_2 are *Ansätze* on n.n.n. bonds. The 8×8 matrix $D_{\mathbf{k}}$ satisfies

$$D_{\mathbf{k}} = -\mu \mathbf{1} + \begin{pmatrix} \mathbf{B}_{\mathbf{k}} & \mathbf{A}_{\mathbf{k}} \\ \mathbf{A}_{\mathbf{k}}^\dagger & \mathbf{B}_{-\mathbf{k}}^T \end{pmatrix}, \quad (26)$$

where $\mathbf{1}$ is the 8×8 identity matrix. The 4×4 matrices $\mathbf{A}_{\mathbf{k}}$ and $\mathbf{B}_{\mathbf{k}}$ have different expression in the 4 gauge-inequivalent states. After a Bogoliubov transformation, the mean-field

Hamiltonian can be diagonalized as

$$H_{\text{MF}} = \sum_{\mathbf{k}\mathbf{s}} \omega_{\mathbf{s}\mathbf{k}} (\gamma_{\mathbf{s}\mathbf{k}\uparrow}^\dagger \gamma_{\mathbf{s}\mathbf{k}\uparrow} + \gamma_{\mathbf{s}\mathbf{k}\downarrow}^\dagger \gamma_{\mathbf{s}\mathbf{k}\downarrow} + 1) + N_c [\mu + \mu\kappa + 8J_1(|A_1|^2 - |B_1|^2) + 2J_2(|A_2|^2 - |B_2|^2)], \quad (27)$$

where $\omega_{\mathbf{s}\mathbf{k}}$ are the spinon dispersions, and $s = 0, 1, 2, 3$. The self-consistent equations for symmetric spin liquid states are

$$16J_1 A_1 = - \sum_s \int_{\text{BZ}} \frac{\partial \omega_{\mathbf{s}\mathbf{k}}}{\partial A_1} d^2k, \quad \text{if } A_1 \neq 0, \quad (28a)$$

$$4J_2 A_2 = - \sum_s \int_{\text{BZ}} \frac{\partial \omega_{\mathbf{s}\mathbf{k}}}{\partial A_2} d^2k, \quad \text{if } A_2 \neq 0, \quad (28b)$$

$$16J_1 B_1 = \sum_s \int_{\text{BZ}} \frac{\partial \omega_{\mathbf{s}\mathbf{k}}}{\partial B_1} d^2k, \quad \text{if } B_1 \neq 0, \quad (28c)$$

$$4J_2 B_2 = \sum_s \int_{\text{BZ}} \frac{\partial \omega_{\mathbf{s}\mathbf{k}}}{\partial B_2} d^2k, \quad \text{if } B_2 \neq 0, \quad (28d)$$

$$1 + \kappa = - \sum_s \int_{\text{BZ}} \frac{\partial \omega_{\mathbf{s}\mathbf{k}}}{\partial \mu} d^2k, \quad (28e)$$

where the integral is over the first Brillouin zone (BZ). With these self-consistent equations, the mean-field *Ansatz* can be solved.

A. (0,0)-flux state

In the $(0,0)$ -flux state, only A_1 and B_2 are nonzero and the configuration is shown in Fig. 15 in Appendix A 2. The $\mathbf{A}_{\mathbf{k}}$ and $\mathbf{B}_{\mathbf{k}}$ of this state are shown in Appendix B 1. After a Bogoliubov transformation, we get the spinon dispersion $\omega_{\mathbf{s}\mathbf{k}}$. Then the mean-field *Ansatz* is solved with the self-consistent equations in Eq. (28). The spinon dispersion at κ_c and the mean-field *Ansatz* amplitudes are shown in Fig. 4.

As shown in Fig. 4(a), the minima of the spinon dispersion is located at $\mathbf{Q} = (\pi, \pi)$, and the gap vanishes at $\kappa = \kappa_c$. When κ is larger than κ_c , the spinon will condense and form a Néel magnetic order. The details of the formation of the magnetic order are discussed in Appendix C. The spinon condenses at the white area in Figs. 4(b) and 4(c), and the contours of the *Ansatz* amplitudes indicate the critical κ_c . We find that κ_c is always smaller than 1 with the change of J_1/J_2 . Therefore, the $(0,0)$ -flux state contributes to the magnetically ordered state in the physical condition. In the condition $\kappa < \kappa_c$, the invariant gauge group of this state is $U(1)$, and this state cannot exist stably and always confines.

B. (0, π)-flux state

In the $(0, \pi)$ -flux state, the *Ansatz* amplitudes A_1 , A_2 , and B_1 are nonzero. The configuration of this state is shown in Fig. 13 in Appendix A 1, and the $\mathbf{A}_{\mathbf{k}}$ and $\mathbf{B}_{\mathbf{k}}$ are shown in Appendix B 2. Diagonalizing the mean-field Hamiltonian by Bogoliubov transformation and solving these self-consistent equations in Eq. (28) we have get the *Ansatz* amplitudes, which are shown in Fig. 5.

With these *Ansatz* values, the spinon dispersion and the structure factor can be obtained, which are shown in Fig. 6. We find the bottom branch of the spinon dispersion is flat; therefore, the critical spinon density κ_c is large in this state.

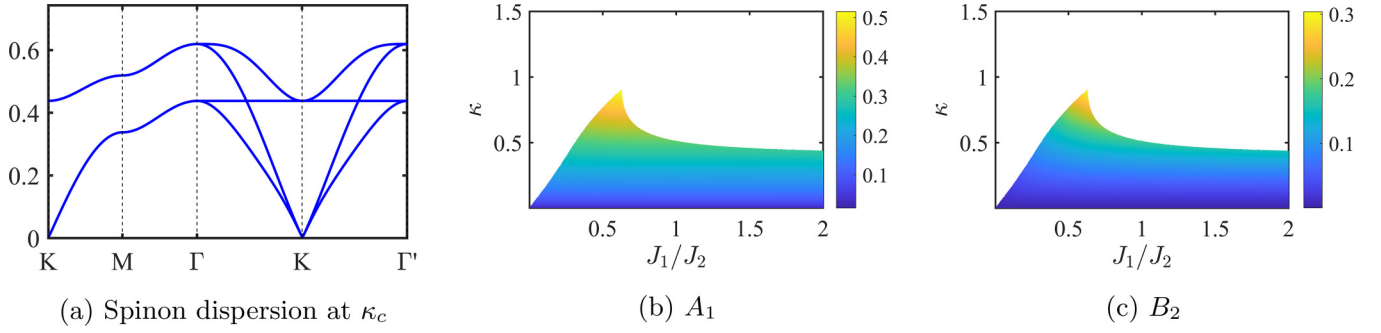


FIG. 4. (a) is the spinon dispersion at $\kappa = \kappa_c$ and $J_1 = J_2 = 1$ of (0,0)-flux state. The plot path is shown in Fig. 2(b). (b) and (c) are the Ansatz A_1 and B_2 value, respectively. A_2 and B_1 are always zero in these two conditions. The spinon condenses at the white area in (b) and (c).

C. $(\pi, 0)$ -flux state

In the $(\pi, 0)$ -flux state, only the Ansatz amplitudes A_1 and B_2 are nonzero, and the configuration is shown in Fig. 16 in Appendix A 2. and the \mathbf{A}_k and \mathbf{B}_k are shown in Appendix B 3. With these self-consistent equations in Eq. (28), the mean-field Ansatz can be solved. The spinon dispersion at physical condition $\kappa = 1$ and the Ansatz amplitudes are shown in Fig. 7.

D. (π, π) -flux state

In the (π, π) -flux state, the Ansatz amplitudes A_1, A_2 , and B_1 are nonzero. The configuration of this state is shown in Fig. 14 in Appendix A 1, and the \mathbf{A}_k and \mathbf{B}_k are shown in Appendix B 4. Solving the self-consistent equations in Eq. (28) we get the Ansatz amplitudes, which are shown in Fig. 8.

With these Ansatz values, the spinon dispersion and the structure factor can be obtained, which are shown in Fig. 9.

As shown in Fig. 9(a), the minimum of the spinon dispersion is located at $\mathbf{Q} = (0, 0)$, and magnetic order will form when $\kappa > \kappa_c$; the details are discussed in Appendix D.

E. Plaquette-singlet states

To study the PS phase, we have tried different Ansatz configurations which break glide symmetries. After solving the self-consistent equations, we find two plaquette-singlet state solutions depicted in Fig. 17. These PS mean-field Ansätze have nonzero A, B amplitudes only in the empty squares or J_2 squares.

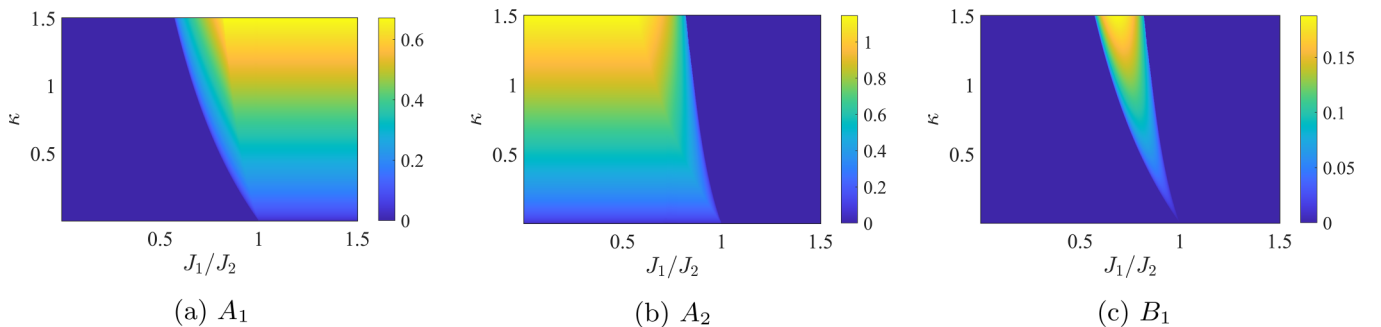


FIG. 5. The Ansatz value (a) A_1 , (b) A_2 , and (c) B_1 of $(0, \pi)$ flux. A_1 is finite at J_1 is large and A_2 is large at J_1 is large. B_1 is finite only when A_1 and A_2 are both finite. B_2 is always zero in this condition.

First we consider the plaquette-singlet state in the empty square. The mean-field Hamiltonian can be written as

$$H_{\text{MF}} = -N_c J_1 \sum_s A_1 \hat{A}_{s,s+1} + \text{H.c.} + 4N_c J_1 \sum_s |A_1|^2 - 4N_c \mu (\hat{n} - \kappa), \quad (29)$$

where the summation is only for the sites in one unit cell, because the mean-field Ansatz is decoupled into disconnected empty squares. The $s = 0, 1, 2, 3$ in this summation is the atom index in the unit cell shown in Fig. 3. After Bogoliubov transformation, the mean-field Hamiltonian is diagonalized as

$$H_{\text{MF}} = N_c \sum_s \omega_s (\gamma_{s\uparrow}^\dagger \gamma_{s\uparrow} + \gamma_{s\downarrow}^\dagger \gamma_{s\downarrow} + 1) + N_c [\mu + \mu\kappa + 4J_1 |A_1|^2], \quad (30)$$

where the spinon dispersions ω_s are

$$\omega_0 = \omega_1 = |\mu|, \quad (31)$$

$$\omega_2 = \omega_3 = \sqrt{\mu^2 - |J_1 A_1|^2}. \quad (32)$$

The self-consistent equations are

$$8J_1 A_1 = - \sum_s \frac{\partial \omega_s}{\partial A_1}, \quad (33)$$

$$1 + \kappa = - \sum_s \frac{\partial \omega_s}{\partial \mu}. \quad (34)$$

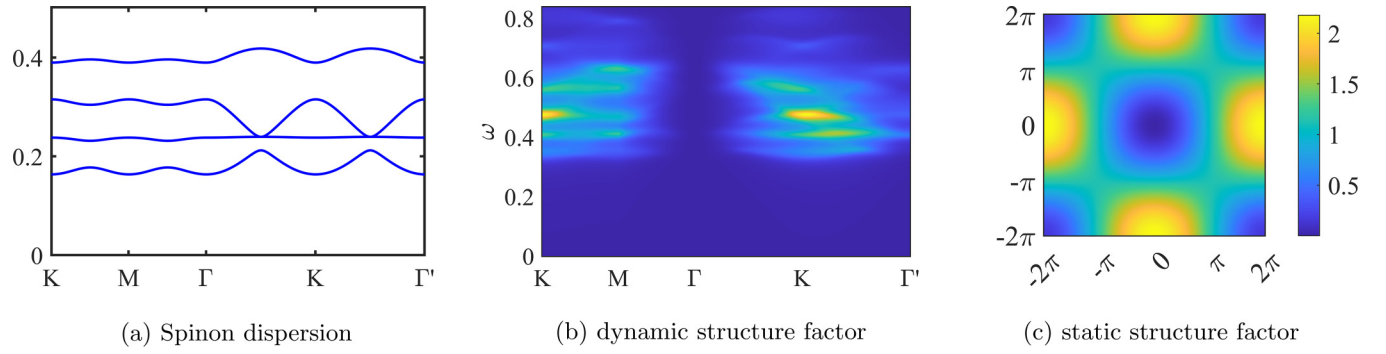


FIG. 6. (a) is the spinon dispersion, (b) is the dynamic structure factor, and (c) is the static structure factor of $(0, \pi)$ -flux state ($J_1/J_2 = 0.7$). The plot path of (a) and (b) is shown in Fig. 2(b).

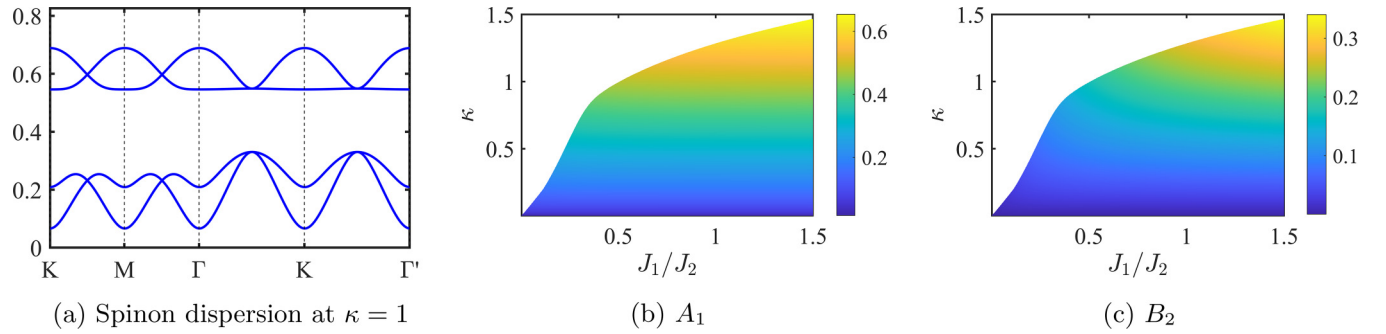


FIG. 7. (a) is the spinon dispersion at $\kappa = \kappa_c$ and $J_1 = J_2 = 1$ of $(\pi, 0)$ flux. The plot path is shown in Fig. 2(b). (b) and (c) are the Ansatz A_1 and B_2 value, respectively. A_2 and B_1 are always zero in this condition.

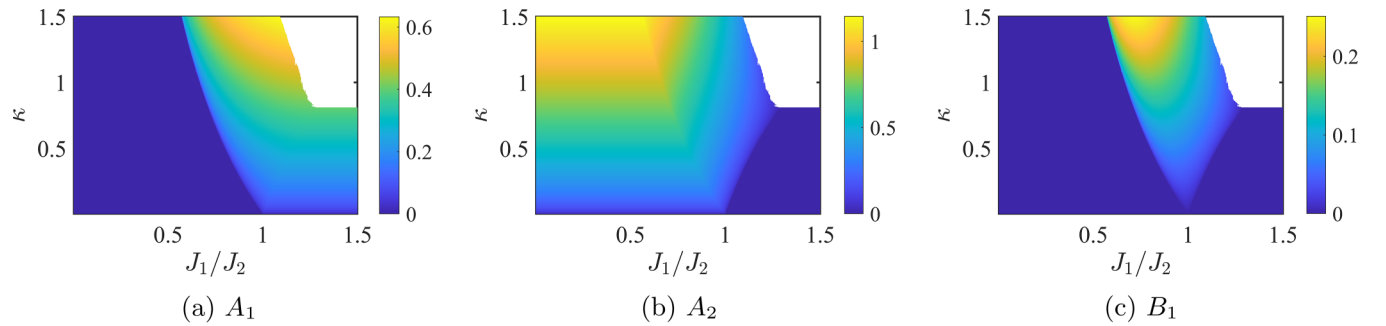


FIG. 8. The Ansatz value (a) A_1 , (b) A_2 , and (c) B_1 of (π, π) flux. A_1 is finite at J_1 is large and A_2 is large at J_1 is large. B_1 is finite only when A_1 and A_2 are both finite. B_2 is always zero in this condition.

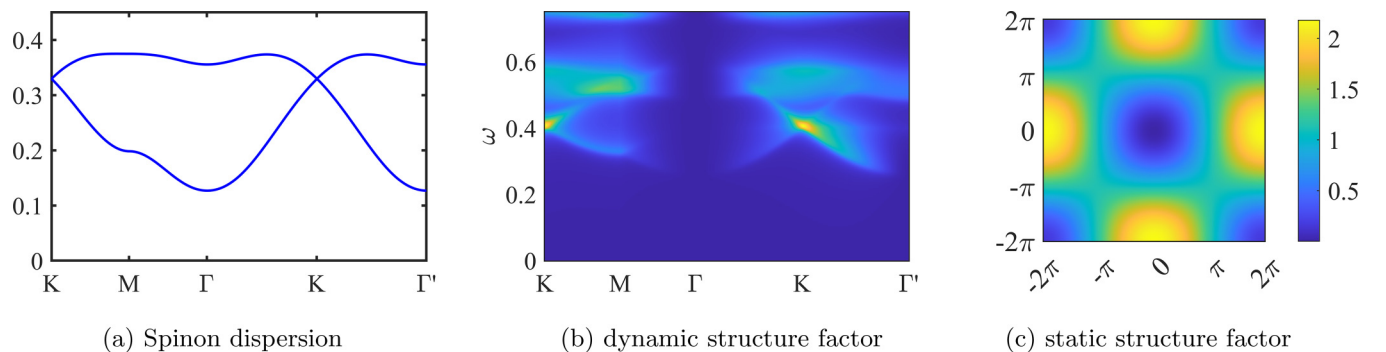


FIG. 9. (a) is the spinon dispersion, (b) is the dynamic structure factor, and (c) is the static structure factor of (π, π) -flux state ($J_1/J_2 = 0.7$). The plot path of (a) and (b) is shown in Fig. 2(b).

Then we consider the plaquette-singlet state in the J_2 square. The mean-field Hamiltonian can be written as

$$H_{\text{MF}} = -N_c J_1 \sum_{\langle ss' \rangle} A_1 \hat{A}_{s,s'} + N_c J_2 B_2 \hat{B}_2 + \text{H.c.} \\ + 4N_c J_1 \sum_s |A_1|^2 - N_c J_2 |B_2|^2 - 4N_c \mu (\hat{n} - \kappa), \quad (35)$$

where s is the index of the sites in the J_2 square and s' is the nearest-neighbor site of the s site in the J_2 square. After Bogoliubov transformation, the mean-field Hamiltonian is diagonalized as

$$H_{\text{MF}} = N_c \sum_s \omega_s (\gamma_{s\uparrow}^\dagger \gamma_{s\uparrow} + \gamma_{s\downarrow}^\dagger \gamma_{s\downarrow} + 1) + N_c [\mu + \mu \kappa \\ + 4J_1 |A_1|^2 - J_2 |B_2|^2], \quad (36)$$

where the spinon dispersions are

$$\omega_0 = |\mu|, \quad (37)$$

$$\omega_1 = \left| \frac{1}{2} J_2 B_2 - \mu \right|, \quad (38)$$

$$\omega_2 = \sqrt{\left(\frac{1}{4} J_2 B_2 + \mu \right)^2 - |J_1 A_1|^2 + \frac{J_2 B_2}{4}}, \quad (39)$$

$$\omega_3 = \sqrt{\left(\frac{1}{4} J_2 B_2 + \mu \right)^2 - |J_1 A_1|^2 - \frac{J_2 B_2}{4}}, \quad (40)$$

and the self-consistent equations are

$$8J_1 A_1 = - \sum_s \frac{\partial \omega_s}{\partial A_1}, \quad (41)$$

$$2J_2 B_2 = \sum_s \frac{\partial \omega_s}{\partial B_2}, \quad (42)$$

$$1 + \kappa = - \sum_s \frac{\partial \omega_s}{\partial \mu}. \quad (43)$$

IV. MEAN-FIELD PHASE DIAGRAM

In the last section we showed the details and results of the four symmetric spin liquid states. The (π, π) - and $(0,0)$ -flux states are called π flux and zero flux hereafter. Comparing the mean-field ground state energies of the 4 gauge-inequivalent symmetric *Ansätze* with the change of J_1/J_2 and κ , we get a mean-field phase diagram of the Heisenberg model in the Shastry-Sutherland lattice, which is shown in Fig. 1(c). We find only two *Ansätze* with zero or π flux in each plaquette as mean-field ground states under physical condition ($\kappa = 1$). The *Ansatz* configurations of these two state are shown in Figs. 10(a) and 10(b).

The zero-flux state is the mean-field ground state for large J_1 ($J_1/J_2 > 0.71$ at $\kappa = 1$). The emergent gauge field for the zero-flux state is a staggered $U(1)$ gauge field, and the spinons are either confined (possibly forming valence bond solid) when κ is small [35] or condensed when κ is large. For physical $\kappa = 1$ the spinons of the zero-flux state condense and form the Néel AFM order. The zero-flux Schwinger boson state and related phases have been discussed before in the context of square lattice antiferromagnets [30].

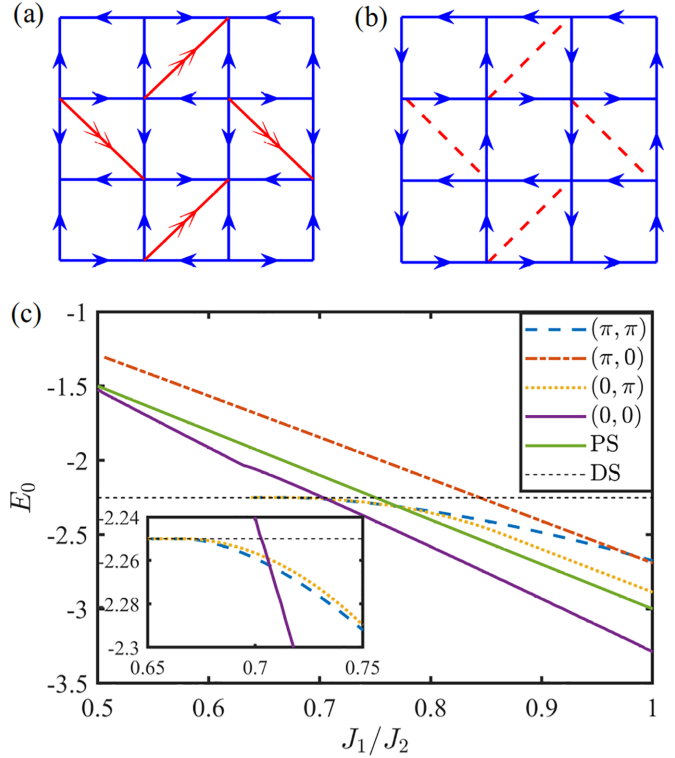


FIG. 10. (a) and (b) are the *Ansätze* A_{ij} of the zero-flux and π -flux states, respectively. An arrow from site i to j means $A_{ij} > 0$ and A_{ij} in dashed lines are zero. The different arrows represent different amplitudes of A_{ij} . (c) is the ground state energies of the 4 gauge-inequivalent symmetric spin liquid *Ansätze* and two valence bound solid (DS and PS) states for $\kappa = 1$. The inset in (c) is the details in $0.65 < J_1/J_2 < 0.75$. It shows that only the DS state and (π, π) -flux and $(0,0)$ -flux SL states appear as mean-field ground states for $\kappa = 1$.

The π -flux state is the mean-field ground state for small J_1 ($J_1/J_2 < 0.71$ at $\kappa = 1$). For intermediate J_1 ($0.66 < J_1/J_2 < 0.71$ at $\kappa = 1$) this state has Z_2 gauge field. For physical $\kappa = 1$ the spinons of this state are gapped and form a gapped Z_2 spin liquid. For very high κ ($\kappa \gtrsim 2.5$ for $J_1/J_2 \sim 0.7$) the bosons will condense and likely form a 4-sublattice antiferromagnetic order similar to the π -flux Schwinger boson state of square lattice antiferromagnets [36].

In the lowest J_1 region ($J_1/J_2 < 0.66$ at $\kappa = 1$) the π -flux state reduces to the confined dimer-singlet state with only next-nearest-neighbor boson pairing $A_2 \neq 0$.

Therefore, there are three distinct phases with the change of J_1/J_2 for physical $\kappa = 1$ under the mean-field approximation: the dimer-singlet phase for $J_1/J_2 < 0.66$, π -flux Z_2 spin liquid state for $0.66 < J_1/J_2 < 0.71$, and Néel phase for $J_1/J_2 > 0.71$. We note that the ground state energy of the $(0, \pi)$ -flux state is slightly higher than the energy of π flux [(π, π) flux] as shown in the inset of Fig. 10(c). Therefore, the $(0, \pi)$ -flux state is not shown in the phase diagram in Fig. 1. However, the energy difference of the (π, π) - and $(0, \pi)$ -flux states is very small. Therefore, this state may also exist beyond the mean-field level.

The dynamic and static structure factors of the π -flux spin liquid state are also calculated by the Schwinger boson mean-field theory and shown in Figs. 9(b) and 9(c), respectively,

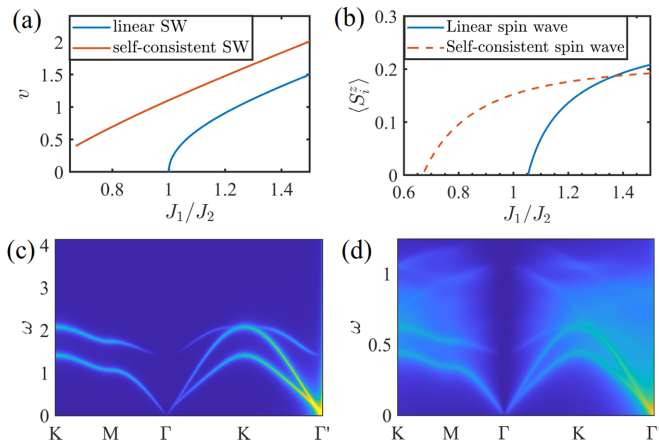


FIG. 11. (a) is the magnon velocity near the Goldstone mode calculated by linear spin wave and self-consistent spin wave theory (see Appendix E). The magnon velocity of linear spin wave vanishes at $J_1/J_2 = 1$, where the magnon dispersion becomes $\propto k^2$ and linear spin wave theory breaks down. (b) is the Néel order parameter computed by self-consistent spin wave theory and linear spin wave theory, which vanishes at $J_1/J_2 \approx 0.65$ and $J_1/J_2 \approx 1.05$, respectively. (c) and (d) are the dynamic structure factor calculated by self-consistent spin wave theory and Schwinger boson mean-field theory in Néel phase. The parameters are $J_1 = 0.9$, $J_2 = 1$.

which may be used as numerical and experimental signatures of this spin liquid state. In particular the dominant short-range spin correlation in this π -flux SL state is related to a 4-sublattice AFM order (see Appendix D).

To further investigate the PS phase, we also study mean-field *Ansätze* with plaquette-singlet order. There are two kinds of plaquette-singlet states for the two kinds of plaquettes in the Shastry-Sutherland lattice. Only the mean-field energy of the plaquette-singlet state in the “empty” square is plotted in Fig. 10(c), because it has lower ground state energy (see Fig. 18 in Appendix A 3). We find that the ground state energy of this state is always higher comparing with the minimum energy of π - and zero-flux SL states with the change of parameter J_1/J_2 , which is shown in Fig. 10(c). However, the energy differences are small near the intermediate region of parameter J_1/J_2 with the π -flux SL ground state. Therefore, the PS state may emerge after considering the gauge fluctuations and projecting the mean-field wave function by Gutzwiller projection, which is beyond the scope of the current work. Because of the absence of the PS state in the mean-field level, the possible DQCP [13,20] cannot be studied by the Schwinger boson mean-field theory.

V. COMPARISON TO SELF-CONSISTENT SPIN WAVE THEORY AND ED

The Néel phase can also be studied by the spin wave theory. However, as shown in Figs. 11(a) and 11(b), the linear spin wave theory breaks down at $J_1/J_2 = 1$ because the spin wave dispersion becomes $\epsilon_k \propto k^2$ under the linear spin wave at $J_1/J_2 = 1$, and the magnetic order parameter for the spin-1/2 model vanishes at $J_1/J_2 = 1.05$, which is much larger than the Néel phase boundary by other theories and numerics. The details of the spin wave dispersion can be referred to

Appendix E. Near the Néel phase boundary, the magnon interactions play important roles and need to be considered. However, the conventional nonlinear spin wave theory by $1/S$ expansion also breaks down near $J_1/J_2 = 1$ because the interaction correction depends on the linear spin wave Hamiltonian. Therefore, we use the self-consistent spin wave theory [37,38] to incorporate the effects of magnon interactions. The idea of the self-consistent spin wave theory is to decouple the quartic terms of Holstein-Primakoff bosons into all possible quadratic terms, and compute these corrections to the linear spin wave Hamiltonian self-consistently. The details of the self-consistent spin wave theory are given in Appendix E. The magnetic order parameter vanishes at $J_1/J_2 \approx 0.65$ by self-consistent spin wave theory as shown in Fig. 11(b), which yields a more accurate Néel phase boundary.

The dynamic structure factors in the Néel phase are calculated to compare the self-consistent spin wave theory and the Schwinger boson mean-field theory. Figures 11(c) and 11(d) are the dynamic structure factors at $J_1/J_2 = 0.9$ calculated by these two theories. In the Néel phase, the Schwinger boson condenses and yields sharp magnon peaks in the dynamic structure factor, while the noncondensing spinons contribute to the continuum. Although the magnon interaction is considered in the self-consistent spin wave theory, the magnon damping channel is not included. Therefore, the magnon peaks are always sharp and there is no continuum in the dynamic structure factor calculated by self-consistent spin wave theory. The dynamic structure factor calculated by self-consistent spin wave theory is more consistent with the Schwinger boson mean-field theory than the linear spin wave theory. We note that the energy scales of dynamic structure factors are different in the Schwinger boson mean-field theory and spin wave theory, and they should become identical in the large- S limit.

We also compare the ground state properties computed by SBMFT and exact diagonalization (see Appendix G). The results are shown in Fig. 12. The ground state from 32-site exact diagonalization is the exact dimer-singlet state for $J_1/J_2 < 0.68$, which is consistent with previous exact-diagonalization studies [11,39] and very close to the SBMFT phase boundary $J_1/J_2 \sim 0.66$ for the DS phase. The nearest-neighbor and next-nearest-neighbor spin correlations also show similar behavior in SBMFT and exact diagonalization. Note that the $\langle S_i \cdot S_j \rangle_{n,n.n.}$ in Fig. 12(e) is -1.25 , which is less than $-3/4$ (the minimal possible value for spin-1/2) in the DS phase. This is due to the spin size (boson number) fluctuation in the mean-field approximation [33].

VI. DISCUSSION AND CONCLUSION

We studied the Shastry-Sutherland model by the Schwinger boson mean-field theory. Using the projective symmetry group method, we find two kinds of possible symmetric *Ansätze*. Comparing the energy of the two *Ansätze* with the change of J_1/J_2 and κ , we get the Schwinger boson mean-field phase diagram of the Shastry-Sutherland model. We find a π -flux gapped Z_2 spin liquid state for the intermediate parameter $0.66 < J_1/J_2 < 0.71$ between the dimer-singlet phase and the Néel AFM phase. This π -flux spin liquid state is continuously connected to the DS phase,

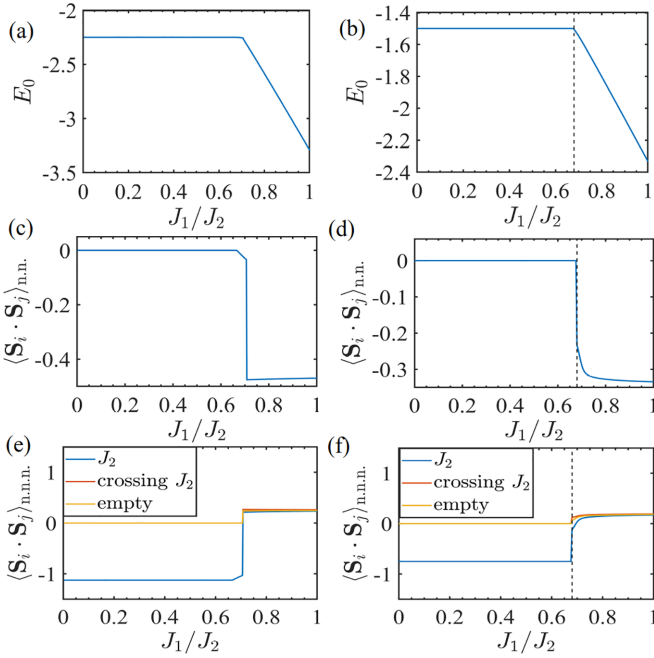


FIG. 12. (a), (c), (e) and (b), (d), (f) are observables calculated by Schwinger boson mean-field theory and 32-site exact diagonalization, respectively. (a) and (b) are the ground state energy per unit cell. (c) and (d) are the nearest-neighbor (n.n.) spin correlation. (e) and (f) are the next-nearest-neighbor (n.n.n.) spin correlation. The Shastry-Sutherland lattice has three inequivalent n.n.n. bonds, which are J_2 bond, bond crossing J_2 bond, and empty bond. The dashed lines in (b), (d), and (f) are $J_1/J_2 = 0.68$. The discontinuity of spin correlation functions and slope of ground state energies at $J_1/J_2 = 0.71$ in (a), (c), (e) indicate that the transition from π -flux spin liquid to Néel order is first order under mean-field approximation, while the transition from DS to π -flux spin liquid at $J_1/J_2 = 0.66$ seems continuous. Note that in (e) $\langle \mathbf{S}_i \cdot \mathbf{S}_j \rangle_{\text{n.n.n.}}$ is less than $-3/4$ (the minimal possible value for spin-1/2) in some parameter range; this is due to the spin size (boson number) fluctuation in the mean-field approximation [33].

but has a first-order transition to the Néel AFM phase upon increasing J_1/J_2 , which can be seen from the discontinuity of spin correlation functions and slope of ground state energies in the Schwinger boson mean-field results in Fig. 12. The continuous transition between the spin liquid and DS phases is an example of the confinement transition of the Ising gauge field [40], which can be described by the condensation of gauge flux excitations (“visons”) and should be dual to an 3D Ising transition. The short-range spin correlation in the π -flux state is closely related to a 4-sublattice AFM order instead of Néel AFM order. We expect that ring-exchange coupling with opposite sign to that derived from the Hubbard model would further stabilize this π -flux spin liquid state [33].

To investigate the possibility of the plaquette-singlet state [12,14,16,18,20–22], we studied PS-ordered *Ansätze* which break the glide symmetry. We found that the ground state energy of these PS-ordered *Ansätze* are higher compared with the symmetric spin liquid *Ansätze* under the mean-field approximation. Therefore, the PS phase does not exist in our mean-field phase diagram. However, the energy difference

between the PS phase and spin liquids is small in the spin liquid phase. So it is possible that the PS phase may emerge after considering gauge fluctuations and Gutzwiller projection of mean-field wave functions, which we leave for future studies.

To further investigate the Néel AFM phase, we used a self-consistent spin wave theory because the linear spin wave theory breaks down for $J_1/J_2 < 1$. The self-consistent spin wave theory renormalizes the magnon dispersion by the magnon interactions, and further stabilizes the magnetic order down to $J_1/J_2 \sim 0.65$. The dynamic structure factor calculated by this theory is more consistent with the results of Schwinger boson mean-field theory except for an overall energy scale.

We have also performed exact diagonalization of the Shastry-Sutherland model with 32 sites. The results indicate that the phase boundary of the dimer-singlet phase is $J_1/J_2 \sim 0.68$, which is roughly consistent with the Schwinger boson mean-field result and previous exact-diagonalization studies of larger system sizes [39]. The behavior of spin correlation functions from the exact-diagonalization results is similar to those of the Schwinger boson mean-field theory, which provides partial support of our mean-field picture of the Shastry-Sutherland model.

Some previous numerical studies [24–26] suggest that the spin liquid phase in the Shastry-Sutherland model is gapless and possibly described by fermionic spinons with Dirac-cone dispersions similar to the DQCP [20]. This gapless spin liquid phase cannot be captured by our Schwinger boson mean-field theory. The possible transition from gapless $U(1)$ spin liquids to gapped Z_2 spin liquids may be studied in controlled large- N approximation [41]. The resulting gapped Z_2 fermionic spinon spin liquid is likely a dual description of the Schwinger boson symmetric Z_2 spin liquids considered here [42], and may be an interesting direction for future theoretical and numerical studies. However it should be noted that the “ π flux” for Abrikosov fermion hoppings in this $U(1)$ spin liquid [20] is not directly related to the “ π flux” of boson pairing terms in our Schwinger boson formalism. In our honest opinion, our Schwinger boson formalism as well as other slave particle formalism are just “phenomenological” low-energy effective theories for quantum spin liquids, that may or may not be realized in a particular model, and should be justified by further numerical and experimental studies.

ACKNOWLEDGMENTS

K.L. thanks F.-Y. Xiong, X.-M. Wang, and J.-R. Xue for helpful discussions. F.W. acknowledges support from the National Natural Science Foundation of China (Grants No. 12274004 and No. 11888101).

APPENDIX A: SOLUTIONS OF THE ALGEBRAIC PSG

In the following we will solve the algebraic PSGs by using these algebraic constraints on the generators of the Shastry-Sutherland lattice space group.

We only consider the condition where the invariant gauge group (IGG) is Z_2 . For a space ground element g , the

Schwinger boson operators are transformed as

$$\hat{b}_{r,s} \rightarrow \exp[i\phi_g(\mathbf{g}\mathbf{r})]\hat{b}_{\mathbf{g}\mathbf{r},s}. \quad (\text{A1})$$

For a defining relation $g_1 g_2 \cdots g_k = \mathbb{1}$, we have

$$\begin{aligned} & \phi_{g_1 g_2 \cdots g_k}(g_1 g_2 \cdots g_k \mathbf{r}) + \phi_{g_2 \cdots g_k}(g_2 \cdots g_k \mathbf{r}) + \cdots + \phi_{g_k}(g_k \mathbf{r}) \\ & = (\text{an IGG element}) = p\pi, \quad p \in \mathbb{Z}_2. \end{aligned} \quad (\text{A2})$$

Note that all these equations about ϕ_s are implicitly modulo 2π .

We consider a gauge transformation $\hat{b}_{r,s} = \exp[i\phi(\mathbf{r})]\hat{b}'_{r,s}$; then the generators of PSG are transformed as

$$\phi'_g(\mathbf{g}\mathbf{r}) = \phi_g(\mathbf{g}\mathbf{r}) + \phi(\mathbf{g}\mathbf{r}) - \phi(\mathbf{r}). \quad (\text{A3})$$

With this relation, by choosing $\phi(X, Y, s)$ for all $X \neq 0$, we can make $\phi'_{T_x}(X, Y, s) = 0$ for all X, Y, s ; then by choosing $\phi(X = 0, Y, s)$, we can make $\phi'_{T_y}(X = 0, Y, s) = 0$ for all Y, s . We are still left three gauge freedoms. The first one is the global constant phase,

$$\phi(X, Y, s)_1 = \phi_s; \quad (\text{A4})$$

this does not change ϕ_{T_x} and ϕ_{T_y} , but will change ϕ_{C_4} and ϕ_σ as

$$\phi'_{C_4}(X, Y, s) = \phi_{C_4}(X, Y, s) + \phi_s - \phi_{s-1}, \quad (\text{A5})$$

$$\phi'_\sigma(X, Y, s) = \phi_\sigma(X, Y, s) + \phi_s - \phi_{-s}. \quad (\text{A6})$$

The second gauge freedom is

$$\phi(X, Y, s)_2 = \pi \cdot X, \quad (\text{A7})$$

which also does not change ϕ_{T_x} and ϕ_{T_y} modulo IGG, but will change ϕ_{C_4} and ϕ_σ as

$$\phi'_{C_4}(X, Y, s) = \phi_{C_4}(X, Y, s) + \pi \cdot (X - Y), \quad (\text{A8})$$

$$\phi'_\sigma(X, Y, s) = \phi_\sigma(X, Y, s) + \pi \cdot (X - Y - x_{-s}). \quad (\text{A9})$$

The third gauge freedom is

$$\phi(X, Y, s)_3 = \pi \cdot (X + Y), \quad (\text{A10})$$

which does not change ϕ_{T_x} and ϕ_{T_y} and ϕ_{C_4} modulo IGG, but will change ϕ_σ as

$$\begin{aligned} \phi'_\sigma(X, Y, s) &= \phi_\sigma(X, Y, s) - \pi \cdot (x_{-s} + y_{-s}) \\ &= \phi_\sigma(X, Y, s) + \pi \cdot s. \end{aligned} \quad (\text{A11})$$

We then consider the relation of the generators of the space group. From the relation of Eq. (12), the algebraic constraint is (ϕ_{T_x} omitted hereafter),

$$\phi_{T_y}(X + 1, Y, s) - \phi_{T_y}(X, Y, s) = p_1\pi; \quad (\text{A12})$$

then the solution is

$$\phi_{T_y}(X, Y, s) = p_1\pi \cdot X. \quad (\text{A13})$$

The algebraic constraint from the relation of Eq. (13) is

$$\begin{aligned} -\phi_{T_y}(X, Y + 1, s) + \phi_{C_4}(X + 1, Y + 1, s) - \phi_{C_4}(X, Y, s) \\ = p_2\pi; \end{aligned} \quad (\text{A14})$$

then we have

$$\phi_{C_4}(X + 1, Y + 1, s) - \phi_{C_4}(X, Y, s) = p_2\pi + p_1\pi \cdot X. \quad (\text{A15})$$

From the relation of Eq. (14), we have

$$\begin{aligned} \phi_{C_4}(X + 1, Y, s) - \phi_{T_y}(Y, -X, s - 1) - \phi_{C_4}(X, Y, s) \\ = p_3\pi, \end{aligned} \quad (\text{A16})$$

which yields

$$\phi_{C_4}(X + 1, Y, s) - \phi_{C_4}(X, Y, s) = p_3\pi + p_1\pi \cdot Y. \quad (\text{A17})$$

Combining with Eq. (A15), the solution is

$$\begin{aligned} \phi_{C_4}(X, Y, s) &= \phi_{C_4}(X, Y, s) + p_2\pi \cdot Y + p_3\pi \cdot (X - Y) \\ &+ p_1\pi \cdot [XY - \frac{1}{2}Y(Y + 1)]. \end{aligned} \quad (\text{A18})$$

Note that we can use the gauge freedom ϕ_2 to set $p_3 = 0$.

From the relation of Eq. (15), the algebraic constraint is

$$\begin{aligned} \phi_{C_4}(X, Y, s) + \phi_{C_4}(Y, -X, s + 3) + \phi_{C_4}(-X, -Y, s + 2) \\ + \phi_{C_4}(-Y, X, s + 1) = p_4\pi, \end{aligned} \quad (\text{A19})$$

from which we have

$$\sum_s \phi_{C_4}(0, 0, s) + p_1\pi \cdot (X^2 + Y^2) = p_4\pi. \quad (\text{A20})$$

Therefore we must have $p_1 = 0$; then $\phi_{T_y}(X, Y, s) = 0$. For simplicity, we define $\phi_{C_4,s} = \phi_{C_4}(0, 0, s)$; then we have the solution

$$\phi_{C_4}(X, Y, s) = p_2\pi \cdot Y + \phi_{C_4,s}, \quad (\text{A21})$$

with $\sum_s \phi_{C_4,s} = p_4\pi$.

The relation of Eq. (16) yields

$$\begin{aligned} \phi_\sigma(X + 1, Y, s) - \phi_{T_y}(-Y + x_{-s}, -X + y_{-s}, -s) \\ - \phi_\sigma(X, Y, s) = p_5\pi; \end{aligned} \quad (\text{A22})$$

then we have

$$\phi_\sigma(X + 1, Y, s) - \phi_\sigma(X, Y, s) = p_5\pi. \quad (\text{A23})$$

Then we consider the relation of Eq. (17), which yields

$$-\phi_{T_y}(X, Y + 1, s) + \phi_\sigma(X, Y + 1, s) - \phi_\sigma(X, Y, s) = p_6\pi; \quad (\text{A24})$$

then we have

$$\phi_\sigma(X, Y + 1, s) - \phi_\sigma(X, Y, s) = p_6\pi. \quad (\text{A25})$$

Combined with Eq. (A23), we get the solution

$$\phi_\sigma(X, Y, s) = \phi_\sigma(0, 0, s) + p_5\pi \cdot X + p_6\pi \cdot Y. \quad (\text{A26})$$

Finally, we consider the relations of Eq. (18) and Eq. (19). The algebraic constraint of Eq. (18) is

$$\phi_\sigma(X, Y, s) - \phi_\sigma(-Y - y_s, -X - x_s, -s) = p_7\pi. \quad (\text{A27})$$

Substituting Eq. (A26) to this equation, we get

$$\begin{aligned} \phi_\sigma(0, 0, s) + \phi_\sigma(0, 0, -s) + (p_5 - p_6)\pi \cdot (X - Y) \\ - p_5\pi y_s - p_3\pi x_s = p_7\pi; \end{aligned} \quad (\text{A28})$$

then we must have $p_5 = p_6$. For simplicity, we define $\phi_{\sigma,s} = \phi_\sigma(0, 0, s)$; then $\phi_\sigma(X, Y, s) = p_5\pi \cdot (X + Y) + \phi_{\sigma,s}$, and $\phi_{\sigma,s} + \phi_{\sigma,-s} = p_7\pi + p_5\pi \cdot s$. The relation Eq. (19) yields

$$\begin{aligned} \phi_{C_4}(X + 1, Y, s) + \phi_\sigma(Y, -X - 1, s - 1) + \phi_{C_4}(X + x_s, \\ -Y - y_s, 1 - s) - \phi_\sigma(X, Y, s) = p_8\pi. \end{aligned} \quad (\text{A29})$$

Substituting Eq. (A21) and (A26), we have

$$\phi_{C_4,s} + \phi_{C_4,1-s} + p_2\pi \cdot (-y_s) + \phi_{\sigma,s-1} - \phi_{\sigma,s} - p_5\pi = p_8\pi, \quad (\text{A30})$$

which yields the following 4 equations by setting the value of s ,

$$\phi_{C_4,0} + \phi_{C_4,1} + \phi_{\sigma,3} - \phi_{\sigma,0} = p_8\pi + p_5\pi, \quad (\text{A31})$$

$$\phi_{C_4,1} + \phi_{C_4,0} + \phi_{\sigma,0} - \phi_{\sigma,1} = p_8\pi + p_5\pi, \quad (\text{A32})$$

$$\phi_{C_4,2} + \phi_{C_4,3} + \phi_{\sigma,1} - \phi_{\sigma,2} = p_8\pi + p_5\pi + p_2\pi, \quad (\text{A33})$$

$$\phi_{C_4,3} + \phi_{C_4,2} + \phi_{\sigma,2} - \phi_{\sigma,3} = p_8\pi + p_5\pi + p_2\pi. \quad (\text{A34})$$

With Eqs. (A31) and (A32), we get $(\phi_{\sigma,3} + \phi_{\sigma,1}) - 2\phi_{\sigma,0} = p_5\pi = 0$; then we have $p_5 = 0$. Then we can set $p_8 = 0$ by using gauge freedom ϕ_3 . With the gauge freedom ϕ_1 , we can also set $\phi_{C_4,1} = \phi_{C_4,2} = \phi_{C_4,3} = 0$; then we have $\phi_{C_4,0} = p_4\pi$. To conclude, the solutions to $\phi_{\sigma,s}$ are (modulo IGG)

$$\phi_{\sigma,0} = \frac{p_7\pi}{2} + p_4\pi, \quad (\text{A35})$$

$$\phi_{\sigma,3} = \frac{p_7\pi}{2}, \quad (\text{A36})$$

$$\phi_{\sigma,1} = \frac{p_7\pi}{2}, \quad (\text{A37})$$

$$\phi_{\sigma,2} = \frac{p_7\pi}{2} + p_2\pi. \quad (\text{A38})$$

Finally, we get the final solution to algebraic PSG:

$$\phi_{T_x}(X, Y, s) = 0, \quad (\text{A39})$$

$$\phi_{T_y}(X, Y, s) = 0, \quad (\text{A40})$$

$$\phi_{C_4}(X, Y, s) = p_2\pi \cdot Y + p_4\pi \cdot \delta_{s,0}, \quad (\text{A41})$$

$$\phi_\sigma(X, Y, s) = \frac{p_7\pi}{2} + p_2\pi \cdot x_s y_s + p_4\pi \cdot \delta_{s,0}, \quad (\text{A42})$$

with three remaining free Z_2 integer parameters p_2, p_4, p_7 . Therefore, there are at most 8 kinds of PSGs.

Then we need to consider the constraints on PSG by *Ansätze*. The n.n. bond poses no constraint, because there is no nontrivial space group element that maps one n.n. bond to itself or its reverse. For the n.n.n. bond, if $A_{n.n.n.} \neq 0$, consider $(0, 0, 0) - (0, -1, 2)$, which is invariant under σ ; then $\phi_\sigma(0, 0, 0) + \phi_\sigma(0, -1, 2) = p_7\pi + p_2\pi + p_4\pi = 0$, namely $p_2 + p_4 + p_7 = 0$; if $B_{n.n.n.} \neq 0$, consider $(0, 0, 0) - (0, -1, 2)$, which is invariant under σ ; then $\phi_\sigma(0, 0, 0) - \phi_\sigma(0, -1, 2) = -p_2\pi - p_4\pi = 0$, namely $p_2 + p_4 = 0$; this is incompatible with $A_{n.n.n.} \neq 0$; consider $(-1, 0, 1) - (0, 0, 3)$, which is reverted by σ ; then $\phi_\sigma(-1, 0, 1) - \phi_\sigma(0, 0, 3) = 0$; then if $B_{n.n.n.} \neq 0$, it must be

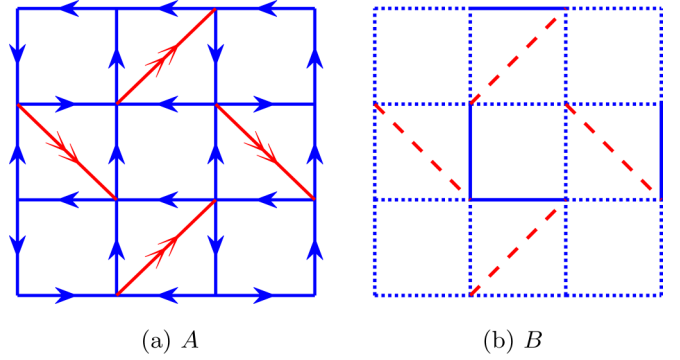


FIG. 13. (a) A . (b) B . The *Ansätze* in dashed lines are 0. The *Ansätze* B are all real and in solid and dotted lines have opposite sign. It is 0 flux in empty squares and π flux in J_2 squares.

real. If we only consider the condition where at least one of $A_{n.n.n.}$ and $B_{n.n.n.}$ is not zero, there are at most 6 kinds of PSGs with these constraints. If we assume the nearest-neighbor *Ansatz* A_1 is nonzero, these 6 states can be classified by two gauge-invariant phases Φ_1 and Φ_2 , which are defined on empty square plaquettes and J_2 square plaquettes, respectively,

$$A_{ij}(-A_{jk}^*)A_{kl}(-A_{li}^*) = |A_1|^4 e^{i\Phi}. \quad (\text{A43})$$

We find that these *Ansätze* with same gauge flux (Φ_1, Φ_2) are gauge equivalent; therefore, we have 4 gauge-inequivalent *Ansätze*. We will show the *Ansätze* and the properties of these 6 kinds of PSGs in the following.

1. $A_{n.n.n.} \neq 0$ and $B_{n.n.n.} = 0$

In this condition, $p_2 + p_4 = 1$ and $p_7 = 1$, and there are two possible *Ansätze*.

For the $(p_2, p_4, p_7) = (1, 0, 1)$ condition, we have the PSG solution,

$$\phi_{T_x}(X, Y, s) = 0, \quad (\text{A44})$$

$$\phi_{T_y}(X, Y, s) = 0, \quad (\text{A45})$$

$$\phi_{C_4}(X, Y, s) = \pi \cdot Y, \quad (\text{A46})$$

$$\phi_\sigma(X, Y, s) = \frac{\pi}{2} + x_s y_s \pi, \quad (\text{A47})$$

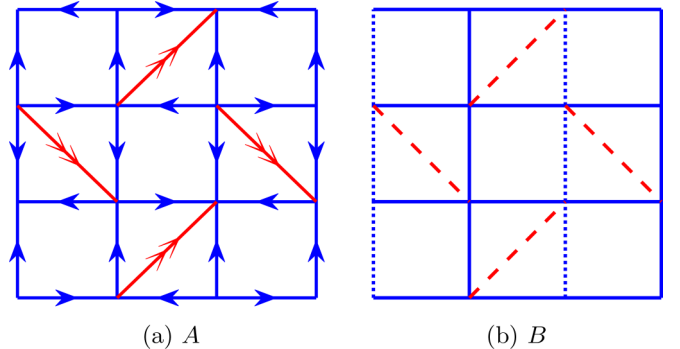


FIG. 14. (a) A . (b) B . The *Ansätze* in dashed lines are 0. The *Ansätze* B are all real and in solid and dotted lines have opposite sign. It is π flux in empty squares and π flux in J_2 squares.

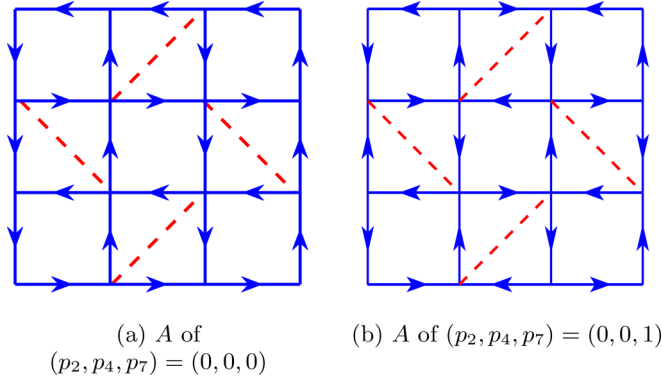


FIG. 15. (a) A of $(p_2, p_4, p_7) = (0, 0, 0)$. (b) A of $(p_2, p_4, p_7) = (0, 0, 1)$. The $Ansätze$ in dashed lines are 0. The two $Ansätze$ are gauge equivalent. It is 0 flux in empty squares and 0 flux in J_2 squares. $B_{n,n} = 0$ and $B_{n,n,n}$ are real and uniform.

from which we get the $(0, \pi)$ -flux $Ansatz$ in this condition, which is shown in Fig. 13. Therefore, after considering the fluctuation of the gauge field and Gutzwiller projection, the $(0, \pi)$ flux may also exist in the phase diagram.

For the $(p_2, p_4, p_7) = (0, 1, 1)$ condition, we have

$$\phi_{T_x}(X, Y, s) = 0, \quad (A48)$$

$$\phi_{T_y}(X, Y, s) = 0, \quad (A49)$$

$$\phi_{C_4}(X, Y, s) = \delta_{s,0}\pi, \quad (A50)$$

$$\phi_{\sigma}(X, Y, s) = \frac{\pi}{2} + \delta_{s,0}\pi. \quad (A51)$$

The $Ansätze$ are the (π, π) flux, which is shown in Fig. 14.

2. $A_{n,n,n} = 0$ and $B_{n,n,n} \neq 0$

In this condition, $p_2 + p_4 = 0$ and there are no constraints on p_7 . Therefore, there are four types of possible $Ansätze$.

First we consider the $p_2 = p_4 = 0$ condition. For the $(p_2, p_4, p_7) = (0, 0, 0)$ condition, the PSG solution is

$$\phi_{C_4}(X, Y, s) = 0, \quad (A52)$$

$$\phi_{\sigma}(X, Y, s) = 0, \quad (A53)$$

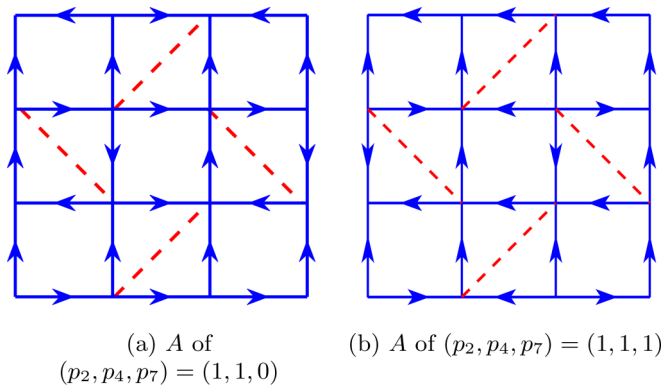


FIG. 16. (a) A of $(p_2, p_4, p_7) = (1, 1, 0)$. (b) A of $(p_2, p_4, p_7) = (1, 1, 1)$. The $Ansätze$ in dashed lines are 0. The two $Ansätze$ are gauge equivalent. It is π flux in empty squares and 0 flux in J_2 squares. $B_{n,n} = 0$ and $B_{n,n,n}$ are real and uniform.

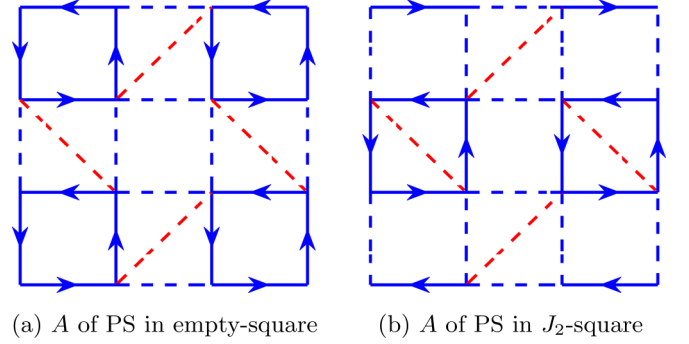


FIG. 17. The $Ansätze$ A of plaquette-singlet state in (a) empty squares and (b) J_2 squares. B of the PS state in empty squares is always zero. For the B of the PS state in J_2 squares, only the B_2 in the J_2 bonds of the J_2 squares is nonzero. $Ansätze$ A in dashed bonds are vanishing in the self-consistent solution.

while $(p_2, p_4, p_7) = (0, 0, 1)$ is

$$\phi_{C_4}(X, Y, s) = 0, \quad (A54)$$

$$\phi_{\sigma}(X, Y, s) = \frac{\pi}{2}. \quad (A55)$$

The $Ansätze$ of these two conditions are both $(0,0)$ flux and gauge equivalent, which are shown in Fig. 15.

Then we consider the $p_2 = p_4 = 1$ condition. For the $(p_2, p_4, p_7) = (1, 1, 0)$ condition, the PSG solution is

$$\phi_{C_4}(X, Y, s) = Y\pi + \delta_{s,0}, \quad (A56)$$

$$\phi_{\sigma}(X, Y, s) = x_s y_s \pi + \delta_{s,0}\pi, \quad (A57)$$

while $(p_2, p_4, p_7) = (1, 1, 1)$ is

$$\phi_{C_4}(X, Y, s) = Y\pi + \delta_{s,0}, \quad (A58)$$

$$\phi_{\sigma}(X, Y, s) = \frac{\pi}{2} + x_s y_s \pi + \delta_{s,0}\pi. \quad (A59)$$

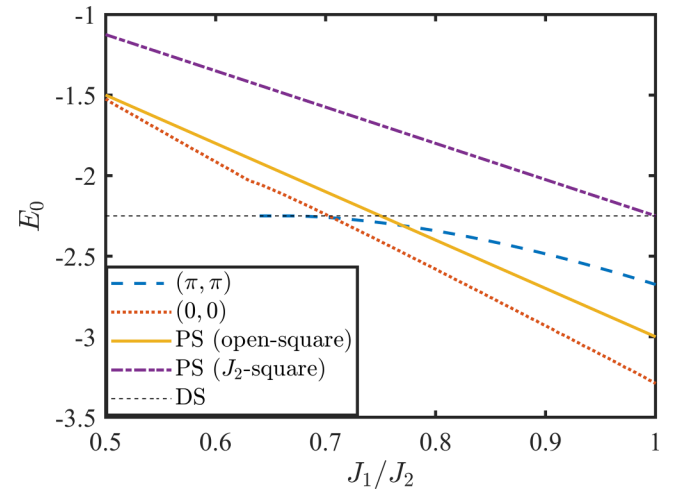


FIG. 18. The mean-field ground state energies in the physical condition $\kappa = 1$. The ground state energy of plaquette-singlet (PS) in the J_2 -square is much larger than that in the empty-square condition because of the existence of B_2 .

The *Ansätze* are both $(\pi, 0)$ flux and also gauge equivalent, which are shown in Fig. 16.

3. Plaquette-singlet state

Now we consider the plaquette-singlet states, which break the glide symmetry and are out of the algebraic PSG solutions. After self-consistent calculation, we find only the zero-flux plaquette-singlet *Ansätze* can be solved self-consistently, and the self-consistent solutions are such that only the *Ansätze* (A and B) within the selected plaquettes are nonzero. Because there are two inequivalent plaquettes (empty square and J_2 square) in the Shastry-Sutherland lattice, only two inequivalent plaquette-singlet *Ansätze* exist, which

are shown in Fig. 17. Calculating the self-consistent equations in Sec. III E, we get the ground state energy with the change of J_1/J_2 . The energies of these two PS states and $(0,0)$ and (π, π) states in physical condition $\kappa = 1$ are shown in Fig. 18.

APPENDIX B: DETAILS OF SCHWINGER BOSON MEAN-FIELD HAMILTONIAN

In the previous section, we showed the mean-field *Ansatz* configurations of the 6 PSGs, which can be classified by 4 gauge-inequivalent solutions. We also showed the configurations of 2 PS states. In this section, we show the Hamiltonian details of the 4 symmetric spin liquid states and 2 PS states.

1. $(0,0)$ -flux state

After Fourier transformation, the mean-field Hamiltonian of the symmetric spin liquids are formally written as Eq. (26). The mean-field configurations of the $(0, \pi)$ -flux state are shown in Fig. 15. Because the two configurations in Fig. 15 are gauge equivalent and have the same physical properties, we just need to consider one of the configurations. If we consider the configuration of Fig. 15(a), the 4×4 matrices $\mathbf{A}_{\mathbf{k}}$ and $\mathbf{B}_{\mathbf{k}}$ of the $(0,0)$ -flux state are

$$\mathbf{A}_{\mathbf{k}} = \begin{pmatrix} 0 & \frac{1}{2}J_1A_1(-1 + e^{-ik_1}) & 0 & \frac{1}{2}J_1A_1(1 - e^{-ik_2}) \\ \frac{1}{2}J_1A_1(1 - e^{ik_1}) & 0 & \frac{1}{2}J_1A_1(-1 + e^{-ik_2}) & 0 \\ 0 & \frac{1}{2}J_1A_1(1 - e^{ik_2}) & 0 & \frac{1}{2}J_1A_1(-1 + e^{ik_1}) \\ \frac{1}{2}J_1A_1(-1 + e^{ik_2}) & 0 & \frac{1}{2}J_1A_1(1 - e^{-ik_1}) & 0 \end{pmatrix}, \quad (\text{B1})$$

$$\mathbf{B}_{\mathbf{k}} = \begin{pmatrix} 0 & 0 & \frac{1}{2}J_2B_2e^{-ik_2} & 0 \\ 0 & 0 & 0 & \frac{1}{2}J_2B_2e^{ik_1} \\ \frac{1}{2}J_2B_2e^{ik_2} & 0 & 0 & 0 \\ 0 & \frac{1}{2}J_2B_2e^{-ik_1} & 0 & 0 \end{pmatrix}. \quad (\text{B2})$$

2. $(0, \pi)$ -flux state

The mean-field configurations of the $(0, \pi)$ -flux state are shown in Fig. 13. The $\mathbf{A}_{\mathbf{k}}$ and $\mathbf{B}_{\mathbf{k}}$ of the $(0,0)$ -flux state are

$$\mathbf{A}_{\mathbf{k}} = \begin{pmatrix} 0 & \frac{1}{2}J_1A_1(-1 - e^{-ik_1}) & -\frac{1}{2}J_2A_2e^{-ik_2} & \frac{1}{2}J_1A_1(1 + e^{-ik_2}) \\ \frac{1}{2}J_1A_1(1 + e^{ik_1}) & 0 & \frac{1}{2}J_1A_1(-1 + e^{-ik_2}) & -\frac{1}{2}J_2A_2e^{ik_1} \\ \frac{1}{2}J_2A_2e^{ik_2} & \frac{1}{2}J_1A_1(1 - e^{ik_2}) & 0 & \frac{1}{2}J_1A_1(-1 + e^{ik_1}) \\ \frac{1}{2}J_1A_1(-1 - e^{ik_2}) & \frac{1}{2}J_2A_2e^{-ik_1} & \frac{1}{2}J_1A_1(1 - e^{-ik_1}) & 0 \end{pmatrix}, \quad (\text{B3})$$

$$\mathbf{B}_{\mathbf{k}} = \begin{pmatrix} 0 & \frac{1}{2}B_1(-1 - e^{-ik_1}) & 0 & \frac{1}{2}B_1(-1 - e^{-ik_2}) \\ \frac{1}{2}B_1(-1 - e^{ik_1}) & 0 & \frac{1}{2}B_1(-1 + e^{-ik_2}) & 0 \\ 0 & \frac{1}{2}B_1(-1 + e^{ik_2}) & 0 & \frac{1}{2}B_1(-1 + e^{ik_1}) \\ \frac{1}{2}B_1(-1 - e^{ik_2}) & 0 & \frac{1}{2}B_1(-1 + e^{-ik_1}) & 0 \end{pmatrix}. \quad (\text{B4})$$

3. $(\pi, 0)$ -flux state

The mean-field configurations of the $(\pi, 0)$ -flux state are shown in Fig. 16. Because the two configurations in Fig. 16 are gauge equivalent and have the same physical properties, we just need to consider one of the configurations. If we consider the configuration of Fig. 16(a), the $\mathbf{A}_{\mathbf{k}}$ and $\mathbf{B}_{\mathbf{k}}$ of the $(\pi, 0)$ -flux state are

$$\mathbf{A}_{\mathbf{k}} = \begin{pmatrix} 0 & \frac{1}{2}J_1A_1(-1 - e^{-ik_1}) & 0 & \frac{1}{2}J_1A_1(-1 - e^{-ik_2}) \\ \frac{1}{2}J_1A_1(1 + e^{ik_1}) & 0 & \frac{1}{2}J_1A_1(-1 + e^{-ik_2}) & 0 \\ 0 & \frac{1}{2}J_1A_1(1 - e^{ik_2}) & 0 & \frac{1}{2}J_1A_1(-1 + e^{ik_1}) \\ \frac{1}{2}J_1A_1(1 + e^{ik_2}) & 0 & \frac{1}{2}J_1A_1(1 - e^{-ik_1}) & 0 \end{pmatrix}, \quad (\text{B5})$$

$$\mathbf{B}_{\mathbf{k}} = \begin{pmatrix} 0 & 0 & \frac{1}{2}J_2B_2e^{-ik_2} & 0 \\ 0 & 0 & 0 & \frac{1}{2}J_2B_2e^{ik_1} \\ \frac{1}{2}J_2B_2e^{ik_2} & 0 & 0 & 0 \\ 0 & \frac{1}{2}J_2B_2e^{-ik_1} & 0 & 0 \end{pmatrix}. \quad (\text{B6})$$

4. (π, π) -flux state

The mean-field configurations of the (π, π) -flux state are shown in Fig. 14. The $\mathbf{A}_{\mathbf{k}}$ and $\mathbf{B}_{\mathbf{k}}$ of the (π, π) -flux state are

$$\mathbf{A}_{\mathbf{k}} = \begin{pmatrix} 0 & \frac{1}{2}J_1A_1(-1 - e^{-ik_1}) & -\frac{1}{2}J_2A_2e^{-ik_2} & \frac{1}{2}J_1A_1(-1 - e^{-ik_2}) \\ \frac{1}{2}J_1A_1(1 + e^{ik_1}) & 0 & \frac{1}{2}J_1A_1(-1 - e^{-ik_2}) & -\frac{1}{2}J_2A_2e^{ik_1} \\ \frac{1}{2}J_2A_2e^{ik_2} & \frac{1}{2}J_1A_1(1 + e^{ik_2}) & 0 & \frac{1}{2}J_1A_1(-1 - e^{ik_1}) \\ \frac{1}{2}J_1A_1(1 + e^{ik_2}) & \frac{1}{2}J_2A_2e^{-ik_1} & \frac{1}{2}J_1A_1(1 + e^{-ik_1}) & 0 \end{pmatrix}, \quad (\text{B7})$$

$$\mathbf{B}_{\mathbf{k}} = \begin{pmatrix} 0 & \frac{1}{2}B_1(1 + e^{-ik_1}) & 0 & \frac{1}{2}B_1(-1 - e^{-ik_2}) \\ \frac{1}{2}B_1(1 + e^{ik_1}) & 0 & \frac{1}{2}B_1(1 + e^{-ik_2}) & 0 \\ 0 & \frac{1}{2}B_1(1 + e^{ik_2}) & 0 & \frac{1}{2}B_1(1 + e^{ik_1}) \\ \frac{1}{2}B_1(-1 - e^{ik_2}) & 0 & \frac{1}{2}B_1(1 + e^{-ik_1}) & 0 \end{pmatrix}. \quad (\text{B8})$$

5. Plaquette-singlet states

The mean-field configurations of the plaquette-singlet states are shown in Fig. 17. It shows that the mean-field *Ansätze* are decoupled into disconnected empty or J_2 squares. In the Nambu spinor $\Psi_{\mathbf{k}} = (b_{0\mathbf{k}\uparrow}, b_{1\mathbf{k}\uparrow}, b_{2\mathbf{k}\uparrow}, b_{3\mathbf{k}\uparrow}, b_{0-\mathbf{k}\downarrow}^\dagger, b_{1-\mathbf{k}\downarrow}^\dagger, b_{2-\mathbf{k}\downarrow}^\dagger, b_{3-\mathbf{k}\downarrow}^\dagger)^T$, the Hamiltonian matrices of the PS states of the open square and J_2 square are

$$H_{\text{open square}} = \begin{pmatrix} -\mu & 0 & 0 & 0 & 0 & -\frac{1}{2}J_1A_1 & 0 & -\frac{1}{2}J_1A_1 \\ 0 & -\mu & 0 & 0 & \frac{1}{2}J_1A_1 & 0 & -\frac{1}{2}J_1A_1 & 0 \\ 0 & 0 & -\mu & 0 & 0 & \frac{1}{2}J_1A_1 & 0 & \frac{1}{2}J_1A_1 \\ 0 & 0 & 0 & -\mu & \frac{1}{2}J_1A_1 & 0 & -\frac{1}{2}J_1A_1 & 0 \\ 0 & \frac{1}{2}J_1A_1 & 0 & \frac{1}{2}J_1A_1 & -\mu & 0 & 0 & 0 \\ -\frac{1}{2}J_1A_1 & 0 & \frac{1}{2}J_1A_1 & 0 & 0 & -\mu & 0 & 0 \\ 0 & -\frac{1}{2}J_1A_1 & 0 & -\frac{1}{2}J_1A_1 & 0 & 0 & -\mu & 0 \\ -\frac{1}{2}J_1A_1 & 0 & \frac{1}{2}J_1A_1 & 0 & 0 & 0 & 0 & -\mu \end{pmatrix}, \quad (\text{B9})$$

$$H_{J_2 \text{ square}} = \begin{pmatrix} -\mu & 0 & 0 & 0 & 0 & -\frac{1}{2}J_1A_1 & 0 & -\frac{1}{2}J_1A_1 \\ 0 & -\mu & 0 & \frac{1}{2}J_2B_2 & \frac{1}{2}J_1A_1 & 0 & -\frac{1}{2}J_1A_1 & 0 \\ 0 & 0 & -\mu & 0 & 0 & \frac{1}{2}J_1A_1 & 0 & \frac{1}{2}J_1A_1 \\ 0 & \frac{1}{2}J_2B_2 & 0 & -\mu & \frac{1}{2}J_1A_1 & 0 & -\frac{1}{2}J_1A_1 & 0 \\ 0 & \frac{1}{2}J_1A_1 & 0 & \frac{1}{2}J_1A_1 & -\mu & 0 & 0 & 0 \\ -\frac{1}{2}J_1A_1 & 0 & \frac{1}{2}J_1A_1 & 0 & 0 & -\mu & 0 & \frac{1}{2}J_2B_2 \\ 0 & -\frac{1}{2}J_1A_1 & 0 & -\frac{1}{2}J_1A_1 & 0 & 0 & -\mu & 0 \\ -\frac{1}{2}J_1A_1 & 0 & \frac{1}{2}J_1A_1 & 0 & 0 & \frac{1}{2}J_2B_2 & 0 & -\mu \end{pmatrix}. \quad (\text{B10})$$

Note that we choose the the J_2 square as the unit cell of $H_{J_2 \text{ square}}$ to get the decoupled Hamiltonian.

APPENDIX C: MAGNETIC ORDER FROM THE ZERO-FLUX STATE

In the Schwinger boson formalism, the magnetic order is formed by the condensation of the Schwinger bosons. When the density of the boson is larger than the critical κ_c , the dispersion of the spinon will become zero at several \mathbf{Q} points, and the spinon will condense at these \mathbf{Q} points and develop magnetic orders.

For the Shastry-Sutherland model, the Néel phase is formed by the condensation of the zero-flux [(0,0)-flux] state. As shown in Fig. 4(a), the dispersion of spinons becomes zero at $\mathbf{Q} = (\pi, \pi)$. Note that $\mathbf{Q} = -\mathbf{Q}$. If we choose the empty square as the unit cell, after Fourier transformation $b_{\mathbf{r}} = \frac{1}{\sqrt{N_c}} \sum_{\mathbf{k}} e^{-i\mathbf{k}\cdot\mathbf{r}} b_{\mathbf{k}}$, the mean-field Hamiltonian becomes

$$H_{\text{MF}} = \sum_{\mathbf{k}} \Psi_{\mathbf{k}}^\dagger D_{\mathbf{k}} \Psi_{\mathbf{k}} + N_c [\mu + \mu\kappa + 8J_1|A_1|^2 - 2J_2|B_2|^2], \quad (\text{C1})$$

where we have used the Nambu spinor $\Psi_{\mathbf{k}} = (b_{0\mathbf{k}\uparrow}, b_{1\mathbf{k}\uparrow}, b_{2\mathbf{k}\uparrow}, b_{3\mathbf{k}\uparrow}, b_{0-\mathbf{k}\downarrow}^\dagger, b_{1-\mathbf{k}\downarrow}^\dagger, b_{2-\mathbf{k}\downarrow}^\dagger, b_{3-\mathbf{k}\downarrow}^\dagger)^T$. The subscript $s = 0, 1, 2, 3$ in $b_{s\mathbf{k}\sigma}$ is the atom index in the unit cell, which is shown in Fig. 3. The 8×8 matrix $D_{\mathbf{k}}$ at \mathbf{Q} is

$$D_{\mathbf{Q}} = \begin{pmatrix} -\mu & 0 & J_2B_2 & 0 & 0 & J_1A_1 & 0 & J_1A_1 \\ 0 & -\mu & 0 & J_2B_2 & -J_1A_1 & 0 & -J_1A_1 & 0 \\ J_2B_2 & 0 & -\mu & 0 & 0 & J_1A_1 & 0 & J_1A_1 \\ 0 & J_2B_2 & 0 & -\mu & -J_1A_1 & 0 & -J_1A_1 & 0 \\ 0 & -J_1A_1 & 0 & -J_1A_1 & -\mu & 0 & J_2B_2 & 0 \\ J_1A_1 & 0 & J_1A_1 & 0 & 0 & -\mu & 0 & J_2B_2 \\ 0 & -J_1A_1 & 0 & -J_1A_1 & J_2B_2 & 0 & -\mu & 0 \\ J_1A_1 & 0 & J_1A_1 & 0 & 0 & J_2B_2 & 0 & -\mu \end{pmatrix}. \quad (\text{C2})$$

In the critical density κ_c , it satisfies

$$-\mu + J_2B_2 - 2A_1 = 0. \quad (\text{C3})$$

At this point, $D_{\mathbf{Q}}$ has two eigenvectors with zero eigenvalue,

$$\begin{aligned} \Psi_1 &= \frac{1}{\sqrt{2}}(0 \ 1 \ 0 \ 1 \ 1 \ 0 \ 1 \ 0)^T, \\ \Psi_2 &= \frac{1}{\sqrt{2}}(-1 \ 0 \ -1 \ 0 \ 0 \ 1 \ 0 \ 1)^T. \end{aligned} \quad (\text{C4})$$

Therefore, the condensation at \mathbf{Q} is $\langle \Psi_{\mathbf{Q}} \rangle = c_1 \Psi_1 + c_2 \Psi_2$, where $c_{1,2}$ are two complex numbers. We define $x_s \equiv (\langle b_{(X,Y,s)\uparrow} \rangle, \langle b_{(X,Y,s)\downarrow} \rangle)^T$; then condensation on site (X, Y, s) is given by

$$\begin{aligned} x_0 = x_2 &= \frac{(-1)^{X+Y}}{\sqrt{2}} \begin{pmatrix} -c_2 \\ c_1^* \end{pmatrix}, \\ x_1 = x_3 &= \frac{(-1)^{X+Y}}{\sqrt{2}} \begin{pmatrix} c_1 \\ c_2^* \end{pmatrix}, \end{aligned} \quad (\text{C5})$$

and the ordered magnetic momentum is then $\mathbf{S}(X, Y, s) = \frac{1}{2} x_s^\dagger \boldsymbol{\sigma} x_s$. Thus we have

$$\mathbf{S}(X, Y, 0) = \mathbf{S}(X, Y, 2) = \mathbf{n}, \quad (\text{C6})$$

$$\mathbf{S}(X, Y, 1) = \mathbf{S}(X, Y, 3) = -\mathbf{n}, \quad (\text{C7})$$

where \mathbf{n} is the $SO(3)$ vector corresponding with the $SU(2)$ vector $(-c_2, c_1^*)^T$. This gives the Néel magnetic order momentum,

$$\mathbf{S}(\mathbf{r}) = (-1)^{\mathbf{r}} \mathbf{n}. \quad (\text{C8})$$

APPENDIX D: MAGNETIC ORDER FROM THE π -FLUX STATE

In the large- κ limit, the spinon in the π -flux spin liquid phase will also condense and form magnetic order. In this section, we discuss the magnetic order from the π -flux state.

The mean-field Hamiltonian of the (π, π) -flux state is

$$\begin{aligned} H_{\text{MF}} &= \sum_{\mathbf{k}} \Psi_{\mathbf{k}}^\dagger D_{\mathbf{k}} \Psi_{\mathbf{k}} + N_c [\mu + \mu\kappa \\ &\quad + 8J_1(|A_1|^2 - |B_1|^2) + 2J_2|A_2|^2], \end{aligned} \quad (\text{D1})$$

where the expression $D_{\mathbf{k}}$ is shown in Eq. (26), and the $\mathbf{A}_{\mathbf{k}}$ and $\mathbf{B}_{\mathbf{k}}$ are shown in Eq. (B5) and Eq. (B6), respectively.

For simplicity, we only discuss the large- J_1 condition, where only A_1 is finite. In the mean-field level, the Shastry-Sutherland lattice is equivalent to the square lattice in this condition where A_2 and B_2 vanish. The magnetic order of this condition is

$$\mathbf{S}(X, Y, 0) = \mathbf{n}_1 + \mathbf{n}_2 + \mathbf{n}_3, \quad (\text{D2})$$

$$\mathbf{S}(X, Y, 1) = -\mathbf{n}_1 + \mathbf{n}_2 - \mathbf{n}_3, \quad (\text{D3})$$

$$\mathbf{S}(X, Y, 2) = -\mathbf{n}_1 - \mathbf{n}_2 + \mathbf{n}_3, \quad (\text{D4})$$

$$\mathbf{S}(X, Y, 3) = \mathbf{n}_1 - \mathbf{n}_2 - \mathbf{n}_3, \quad (\text{D5})$$

which is discussed in Ref. [36], and $n_1^2 + n_2^2 + n_3^2 = n^2$. The details of the calculation can be referred to Appendix C in Ref. [36].

APPENDIX E: SELF-CONSISTENT SPIN WAVE THEORY

In this section, we introduce the self-consistent spin wave theory in detail. Near the phase boundary of the Néel phase, the quantum fluctuation is significant and the interaction of

magnons takes an important role. For the Shastry-Sutherland model, the linear spin wave Hamiltonian is not positive or semipositive definite in $J_1/J_2 < 1$, and the linear spin wave theory breaks down in this region. The nonlinear spin wave theory also breaks down because the correction of the magnon interaction depends on the magnon wave function of linear spin wave theory. Therefore, we need to use a self-consistent spin wave theory to study the Néel phase of the Shastry-Sutherland model in $J_1/J_2 < 1$.

Spin wave theory is to describe the ordered phase in terms of small fluctuations of the spins about their expectation values, which can be regarded as the classical ground state of the Hamiltonian. For the Shastry-Sutherland model, the magnetic ordered state is a Néel state, and the classical ground state is the Néel antiferromagnetic state. With the classical ground

state, the spin Hamiltonian can be expressed by the boson operators by the Holstein-Primakoff transformation [43]. Expanding the Hamiltonian by $1/S$ as we regarding S as a large number, the Hamiltonian is transformed to

$$H = H_0 + H_2 + H_4 + H_6 + \dots, \quad (\text{E1})$$

where the linear term H_1 vanishes if the classical ground state is proper. Keeping up to quadratic terms H_2 , one obtains the noninteracting spin wave Hamiltonian. The higher-order terms $H_4 + H_6 + \dots$ introduce the interactions of magnons. For the Shastry-Sutherland model, if we choose the “ J_2 square” as the unit cell, the linear spin wave Hamiltonian H_2 in the momentum space can be written as

$$H_2 = \sum_k (a_k^\dagger \quad b_k^\dagger \quad c_k^\dagger \quad d_k^\dagger \quad a_{-k} \quad b_{-k} \quad c_{-k} \quad d_{-k}) \mathcal{H}_k \begin{pmatrix} a_k \\ b_k \\ c_k \\ d_k \\ a_{-k}^\dagger \\ b_{-k}^\dagger \\ c_{-k}^\dagger \\ d_{-k}^\dagger \end{pmatrix}; \quad (\text{E2})$$

here a, b, c, d are the Holstein-Primakoff bosons for the unit cell that has 4 sites. The \mathcal{H}_k satisfies

$$\mathcal{H}_k = \begin{pmatrix} \mathbf{B}_k & \mathbf{A}_k \\ \mathbf{A}_k^\dagger & \mathbf{B}_{-k}^T \end{pmatrix}, \quad (\text{E3})$$

$$\mathbf{A}_k = \begin{pmatrix} 0 & \frac{1}{2}J_1(1 + e^{ik_1}) & 0 & \frac{1}{2}J_1(1 + e^{ik_2}) \\ \frac{1}{2}J_1(1 + e^{-ik_1}) & 0 & \frac{1}{2}J_1(1 + e^{ik_2}) & 0 \\ 0 & \frac{1}{2}J_1(1 + e^{-ik_2}) & 0 & \frac{1}{2}J_1(1 + e^{-ik_1}) \\ \frac{1}{2}J_1(1 + e^{-ik_2}) & 0 & \frac{1}{2}J_1(1 + e^{ik_1}) & 0 \end{pmatrix}, \quad (\text{E4})$$

$$\mathbf{B}_k = \begin{pmatrix} 2J_1 - \frac{1}{2}J_2 & 0 & 0 & 0 \\ 0 & 2J_1 - \frac{1}{2}J_2 & 0 & \frac{1}{2}J_2 e^{i(k_1 - k_2)} \\ 0 & 0 & 2J_1 - \frac{1}{2}J_2 & 0 \\ 0 & \frac{1}{2}J_2 e^{i(-k_1 + k_2)} & 0 & 2J_1 - \frac{1}{2}J_2 \end{pmatrix}. \quad (\text{E5})$$

Using Bogoliubov transformation to diagonalize the \mathcal{H}_k , we will get the linear spin wave dispersion and wave functions, which break down at $J_1/J_2 < 1$. The self-consistent spin wave theory is to use the boson-pair expectation values to decouple the quartic terms. We use a specific term for example:

$$\begin{aligned} \sum_{k,p,q} V(\mathbf{k}, \mathbf{p}, \mathbf{q}) a_k^\dagger b_p^\dagger a_q b_{k+p-q} &\approx \sum_k \left[\sum_{p,q} V(\mathbf{k}, \mathbf{p}, \mathbf{k}) \langle b_p^\dagger b_p \rangle \right] a_k^\dagger a_k + \dots \\ &= \sum_k f(\mathbf{k}) a_k^\dagger a_k + \dots \end{aligned} \quad (\text{E6})$$

Here a and b are the boson operators of different flavors, and we set $\sum_{\mathbf{k}} f(\mathbf{k}) \equiv \sum_{p,q} V(\mathbf{k}, \mathbf{p}, \mathbf{k}) \langle b_p^\dagger b_p \rangle$. The symbol (\dots) represents the other decoupling types. Therefore, the Hamiltonian is transformed into

$$\begin{aligned} H &= H_2 + H_4 + \dots \\ &= H_2 + \tilde{H}_2 + H_4 - \tilde{H}_2 + \dots \\ &= H'_2 + H'_4, \end{aligned} \quad (\text{E7})$$

and $H'_4 = 0$ in the mean-field level. We call this theory a self-consistent spin wave theory because the decoupled quartic term \tilde{H}_2 needs to be calculated self-consistently. The effects of magnon interaction are considered in this theory. When H_2 is not positive or semipositive definite, this method may also work because we only need to keep H'_2 to be positive and semipositive definite. For the Shastry-Sutherland model, the self-consistent spin wave theory works in the $J_1/J_2 > 0.65$, where the magnetic order parameter vanishes, which indicates the phase boundary of the Néel state.

APPENDIX F: CONTINUUM LIMIT OF LINEAR SPIN WAVE ON SHASTRY-SUTHERLAND MODEL

In this section, we follow the prescription in Refs. [44] to derive the continuum field theory of the linear spin wave on the Shastry-Sutherland model. The magnon velocity can be obtained from this continuum field theory.

We assume the Néel order is along the z direction,

$$\langle S_i \rangle = (-1)^s S \hat{z}; \quad (\text{F1})$$

here $s = 0, 1, 2, 3$, which is the sublattice label shown in Fig. 3. The lattice vectors are $2\hat{x}$ and $2\hat{y}$. The site position in the Shastry-Sutherland lattice is expressed by (\mathbf{r}, s) , where \mathbf{r} is the unit cell position and s is the sublattice label. After Holstein-Primakoff transformation, the linear spin wave

Hamiltonian is

$$\begin{aligned} H_{LSW} &= S \sum_{\mathbf{r}} \left\{ (4J_1 - J_2) \sum_s b_{s\mathbf{r}}^\dagger b_{s\mathbf{r}} \right. \\ &\quad + J_2 (b_{1\mathbf{r}}^\dagger b_{3\mathbf{r}+\hat{x}+\hat{y}} + b_{0\mathbf{r}}^\dagger b_{2\mathbf{r}+\hat{x}-\hat{y}} + \text{H.c.}) \\ &\quad - J_1 [b_{0\mathbf{r}} (b_{1\mathbf{r}+\hat{x}} + b_{1\mathbf{r}-\hat{x}} + b_{3\mathbf{r}+\hat{y}} + b_{3\mathbf{r}-\hat{y}}) \\ &\quad \left. + b_{2\mathbf{r}} (b_{1\mathbf{r}+\hat{y}} + b_{1\mathbf{r}-\hat{y}} + b_{3\mathbf{r}+\hat{x}} + b_{3\mathbf{r}-\hat{x}}) + \text{H.c.}] \right\}. \end{aligned} \quad (\text{F2})$$

In the imaginary-time path-integral formalism, the bosonic $b_{s\mathbf{r}}$ operators become complex fields. For later convenience, the operators are transformed to complex fields as

$$b_{0\mathbf{r}} \rightarrow \phi_0(\mathbf{r}), \quad (\text{F3})$$

$$b_{1\mathbf{r}} \rightarrow \phi_1^*(\mathbf{r}), \quad (\text{F4})$$

$$b_{2\mathbf{r}} \rightarrow \phi_2(\mathbf{r}), \quad (\text{F5})$$

$$b_{3\mathbf{r}} \rightarrow \phi_3^*(\mathbf{r}). \quad (\text{F6})$$

The gradient expansion is used to get the continuum field theory from the linear spin wave Hamiltonian in Eq. (F2),

$$\begin{aligned} &\phi_s^*(\mathbf{r}) \phi_{s'}(\mathbf{r} + \mathbf{a}) \\ &= \phi_s^*(\mathbf{r}) \left[\phi_{s'}(\mathbf{r}) + \mathbf{a} \cdot \nabla_{\mathbf{r}} \phi_{s'}(\mathbf{r}) + \frac{1}{2} (\mathbf{a} \cdot \nabla_{\mathbf{r}})^2 \phi_{s'}(\mathbf{r}) + \dots \right]. \end{aligned} \quad (\text{F7})$$

Substituting the gradient expansion to the linear spin wave Hamiltonian and keeping up to the 2nd order, we obtain the Hamiltonian density,

$$\mathcal{H} = \mathcal{H}_0 + \mathcal{H}_1 + \mathcal{H}_2; \quad (\text{F8})$$

here \mathcal{H}_0 has no gradient, \mathcal{H}_1 has the 1st-order gradient terms, and \mathcal{H}_2 has the 2nd-order gradient terms. The expression of \mathcal{H}_0 is

$$\mathcal{H}_0 = (\phi_0^*(\mathbf{r}) \quad \phi_1^*(\mathbf{r}) \quad \phi_2^*(\mathbf{r}) \quad \phi_3^*(\mathbf{r})) \begin{pmatrix} 4J_1 - J_2 & -2J_1 & J_2 & -2J_1 \\ -2J_1 & 4J_1 - J_2 & -2J_1 & J_2 \\ J_2 & -2J_1 & 4J_1 - J_2 & -2J_1 \\ -2J_1 & J_2 & -2J_1 & 4J_1 - J_2 \end{pmatrix} \begin{pmatrix} \phi_0(\mathbf{r}) \\ \phi_1(\mathbf{r}) \\ \phi_2(\mathbf{r}) \\ \phi_3(\mathbf{r}) \end{pmatrix}, \quad (\text{F9})$$

and the eigenvalues and eigenvectors of \mathcal{H}_0 are

$$\begin{aligned} 0, \Psi_0 &= \begin{pmatrix} 1/2 \\ 1/2 \\ 1/2 \\ 1/2 \end{pmatrix}; & 8J_1 S, \Psi_1 &= \begin{pmatrix} 1/2 \\ -1/2 \\ 1/2 \\ -1/2 \end{pmatrix}; \\ (4J_1 - 2J_2)S, \Psi_2 &= \begin{pmatrix} 1/2 \\ 1/2 \\ -1/2 \\ -1/2 \end{pmatrix}; & (4J_1 - 2J_2)S, \Psi_3 &= \begin{pmatrix} 1/2 \\ -1/2 \\ -1/2 \\ 1/2 \end{pmatrix}. \end{aligned} \quad (\text{F10})$$

The eigenvector Ψ_0 with zero eigenvalue is the Goldstone mode. Then the \mathcal{H}_0 is diagonalized as

$$\mathcal{H}_0 = 8SJ_1\Psi_1^*\Psi_1 + S(4J_1 - 2J_2)(\Psi_2^*\Psi_2 + \Psi_3^*\Psi_3). \quad (\text{F11})$$

For later convenience, we set $\phi \equiv (\phi_0(\mathbf{r}) \ \phi_1(\mathbf{r}) \ \phi_2(\mathbf{r}) \ \phi_3(\mathbf{r}))^T$ and $\Psi \equiv (\Psi_0(\mathbf{r}) \ \Psi_1(\mathbf{r}) \ \Psi_2(\mathbf{r}) \ \Psi_3(\mathbf{r}))^T$. The expression of \mathcal{H}_1 is

$$\begin{aligned} \mathcal{H}_1 &= SJ_2[\phi_1(\partial_x + \partial_y)\phi_3^* + \phi_0^*(\partial_x - \partial_y)\phi_2 - \phi_3(\partial_x + \partial_y)\phi_1^* - \phi_2^*(\partial_x - \partial_y)\phi_0] \\ &= SJ_2 \left[\phi^* \begin{pmatrix} 0 & 0 & 1 & 0 \\ 0 & 0 & 0 & 1 \\ -1 & 0 & 0 & 0 \\ 0 & -1 & 0 & 0 \end{pmatrix} \partial_x \phi + \phi^* \begin{pmatrix} 0 & 0 & -1 & 0 \\ 0 & 0 & 0 & 1 \\ 1 & 0 & 0 & 0 \\ 0 & -1 & 0 & 0 \end{pmatrix} \partial_y \phi \right] \\ &= SJ_2 \left[\Psi^* \begin{pmatrix} 0 & 0 & -1 & 0 \\ 0 & 0 & 0 & -1 \\ 1 & 0 & 0 & 0 \\ 0 & 1 & 0 & 0 \end{pmatrix} \partial_x \Psi + \Psi^* \begin{pmatrix} 0 & 0 & 0 & -1 \\ 0 & 0 & -1 & 0 \\ 0 & 1 & 0 & 0 \\ 1 & 0 & 0 & 0 \end{pmatrix} \partial_y \Psi \right]. \quad (\text{F12}) \end{aligned}$$

Now we consider the 2nd-order gradient terms \mathcal{H}_2 , whose expression is

$$\begin{aligned} \mathcal{H}_2 &= \frac{1}{2}SJ_2[\phi_1(\partial_x + \partial_y)^2\phi_3^* + \phi_0(\partial_x - \partial_y)^2\phi_2^* \\ &\quad + \phi_3(\partial_x + \partial_y)^2\phi_1^* + \phi_2(\partial_x - \partial_y)^2\phi_0^*] \\ &\quad - SJ_1[\phi_0(\partial_x^2\phi_1^* + \partial_y^2\phi_3^*) + \phi_2(\partial_y^2\phi_1^* + \partial_x^2\phi_3^*) + \text{c.c.}]. \quad (\text{F13}) \end{aligned}$$

In the continuum limit, the low-energy effective theory is only contributed by the Goldstone mode Ψ_0 . Therefore, we need to integrate the high-energy modes Ψ_1, Ψ_2 , and Ψ_3 to get the effective field theory of Ψ_0 . For this purpose, we only keep the $\Psi_0^*(\dots)\Psi_0$ terms in \mathcal{H}_2 because the other terms in \mathcal{H}_2 do not contribute the effective field theory of Ψ_0 up to 2nd-order

gradient terms. Then we just need to replace ϕ_s by $\frac{1}{2}\Psi_0$,

$$\begin{aligned} \mathcal{H}_2 &\cong \frac{1}{4}SJ_2[\Psi_0(\partial_x + \partial_y)^2\Psi_0^* + \Psi_0(\partial_x - \partial_y)^2\Psi_0^*] \\ &\quad - \frac{1}{2}SJ_1[\Psi_0(\partial_x^2 + \partial_y^2)\Psi_0^* + \Psi_0^*(\partial_x^2 + \partial_y^2)\Psi_0] + \dots \\ &= S(J_1 - \frac{1}{2}J_2)[(\partial_x\Psi_0^*)(\partial_x\Psi_0) + (\partial_y\Psi_0^*)(\partial_y\Psi_0)]. \quad (\text{F14}) \end{aligned}$$

The Lagrangian density of the linear spin wave theory is

$$\begin{aligned} \mathcal{L} &= \phi_0^*\partial_\tau\phi_0 - \phi_1^*\partial_\tau\phi_1 + \phi_2^*\partial_\tau\phi_2 - \phi_3^*\partial_\tau\phi_3 - \mathcal{H} \\ &= \Psi_0^*\partial_\tau\Psi_1 + \Psi_1^*\partial_\tau\Psi_0 + \Psi_2^*\partial_\tau\Psi_3 + \Psi_3^*\partial_\tau\Psi_2 - \mathcal{H}. \quad (\text{F15}) \end{aligned}$$

By integrating the high-energy modes by the Gaussian part of their action in \mathcal{H} , we get the effective action for Ψ_0 , whose Lagrangian density is

$$\begin{aligned} \mathcal{L}_{\text{eff}} &= \frac{1}{8SJ_1}(\partial_\tau\Psi_0^*)(\partial_\tau\Psi_0) + S \left[J_1 - \frac{J_2}{2} - \frac{J_2^2}{4J_1 - 2J_2} \right] \\ &\quad \times [(\partial_x\Psi_0^*)(\partial_x\Psi_0) + (\partial_y\Psi_0^*)(\partial_y\Psi_0)], \quad (\text{F16}) \end{aligned}$$

which yields the dispersion relation

$$\frac{1}{8SJ_1}\omega^2 = S \left[J_1 - \frac{J_2}{2} - \frac{J_2^2}{4J_1 - 2J_2} \right] \mathbf{k}^2. \quad (\text{F17})$$

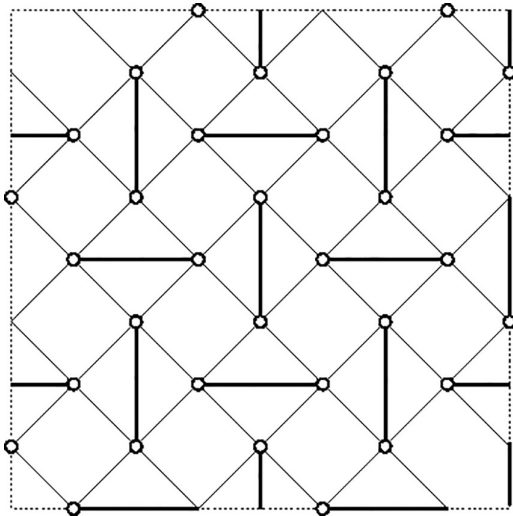


FIG. 19. The 32-site Shastry-Sutherland lattice used in the ED study. Open circles indicate distinct sites under periodic boundary condition. J_2 and J_1 bonds are depicted as thick and thin solid lines, respectively.

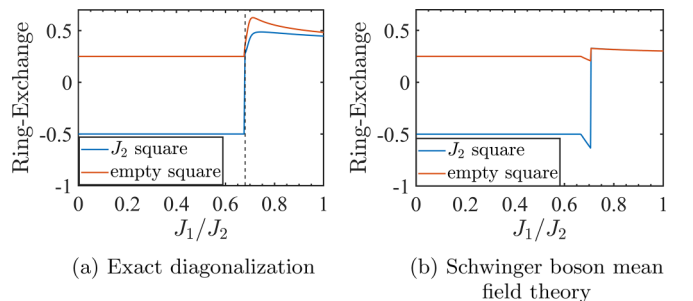


FIG. 20. Expectation values of 4-site ring exchange operators around “ J_2 square” and “empty square” calculated by (a) exact diagonalization and (b) Schwinger boson mean-field theory.

TABLE I. Magnon velocities and magnetic moment sizes from self-consistent spin wave (SCSW) and linear spin wave (LSW). The unit of the velocities is $J_2 a$, where a is the square lattice constant. The magnetic moment is calculated by $1/2 - \langle n_m \rangle$, where $\langle n_m \rangle$ is the average magnon density. “n.a.” means not applicable.

J_1/J_2	0.7	0.75	0.8	0.85	0.9	0.95	1	1.05	1.1	1.15	1.2	1.25	1.13	1.35	1.4
v_{SCSW}	0.470	0.585	0.695	0.802	0.905	1.005	1.103	1.199	1.294	1.387	1.478	1.569	1.659	1.748	1.836
v_{LSW}	n.a.	n.a.	n.a.	n.a.	n.a.	n.a.	0	0.447	0.635	0.781	0.907	1.021	1.126	1.225	1.320
m_{SCSW}	0.032	0.069	0.096	0.116	0.130	0.143	0.153	0.160	0.166	0.171	0.176	0.180	0.183	0.186	0.188
m_{LSW}	n.a.	n.a.	n.a.	n.a.	n.a.	n.a.	n.a.	n.a.	0.067	0.109	0.136	0.156	0.171	0.183	0.193

Finally, we get the magnon velocity v_{sw} of linear spin wave theory,

$$v_{\text{sw}} = 4SJ_1 \sqrt{\frac{J_1 - J_2}{2J_1 - J_2}}, \quad (\text{F18})$$

which vanishes at $J_1 = J_2$, where the linear spin wave theory breaks down. For the magnon velocity of the self-consistent spin wave theory, it can only be calculated numerically. The magnon velocities and magnetic moment sizes calculated by self-consistent and linear spin wave theory are shown in Table I.

APPENDIX G: EXACT DIAGONALIZATION OF 32-SITE SHASTRY-SUTHERLAND MODEL

We study the ground state properties of the Shastry-Sutherland model [see Eq. (1)] by exact diagonalization, on a finite-size ($2\sqrt{2} \times 2\sqrt{2} \times 4$) lattice with 32 sites (see Fig. 19). With periodic boundary conditions this preserves the full lattice symmetries of the Shastry-Sutherland model.

The ground state energies and wave functions are obtained by the Lanczos method. The following lattice symmetries

are exploited to reduce the Hilbert space sizes: (a) lattice translations (with respect to 4-site unit cell), and (b) four-fold rotation C_4 around the center of an empty square, in the translation trivial sector. The ground states are found in the sector with trivial translations and C_4 eigenvalue (+1). The reduced Hilbert space size is 18 788 230 for this 32-site lattice.

We consider antiferromagnetic J_1 and J_2 couplings and set $J_2 = 1$. The ground state energy and some of the ground state spin-spin correlation functions are shown in Fig. 12. We note that for $J_1/J_2 \leq 0.67578125$ the exact ground state is the dimer-singlet state, and a level crossing happens for J_1/J_2 between 0.67578125 and 0.677734375. This level crossing point is consistent with previous exact-diagonalization studies [25].

Here we also present the ground state expectation values of the 4-site ring exchange operators around “ J_2 square” and “empty square” from the exact diagonalization, and compare them to the Schwinger boson mean-field theory results (see Fig. 20). This operator cyclically permutes spins on the four sites involved; namely it is $\sum_{\{s_i\}} (|s_1, s_2, s_3, s_4\rangle \langle s_2, s_3, s_4, s_1| + \text{H.c.})$.

- [1] Y. Cui, L. Liu, H. Lin, K.-H. Wu, W. Hong, X. Liu, C. Li, Z. Hu, N. Xi, S. Li, R. Yu, A. W. Sandvik, and W. Yu, Proximate deconfined quantum critical point in $\text{SrCu}_2(\text{BO}_3)_2$, *Science* **380**, 1179 (2023).
- [2] M. E. Zayed, C. Rüegg, J. Larrea J., A. M. Läuchli, C. Panagopoulos, S. S. Saxena, M. Ellerby, D. F. McMorrow, T. Strässle, S. Klotz, G. Hamel, R. A. Sadykov, V. Pomjakushin, M. Boehm, M. Jiménez-Ruiz, A. Schneidewind, E. Pomjakushina, M. Stingaciu, K. Conder, and H. M. Rønnow, 4-spin plaquette singlet state in the Shastry-Sutherland compound $\text{SrCu}_2(\text{BO}_3)_2$, *Nat. Phys.* **13**, 962 (2017).
- [3] J. Guo, G. Sun, B. Zhao, L. Wang, W. Hong, V. A. Sidorov, N. Ma, Q. Wu, S. Li, Z. Y. Meng, A. W. Sandvik, and L. Sun, Quantum phases of $\text{SrCu}_2(\text{BO}_3)_2$ from high-pressure thermodynamics, *Phys. Rev. Lett.* **124**, 206602 (2020).
- [4] J. L. Jiménez, S. P. G. Crone, E. Fogh, M. E. Zayed, R. Lortz, E. Pomjakushina, K. Conder, A. M. Läuchli, L. Weber, S. Wessel, A. Honecker, B. Normand, C. Rüegg, P. Corboz, H. M. Rønnow, and F. Mila, A quantum magnetic analogue to the critical point of water, *Nature (London)* **592**, 370 (2021).
- [5] T. Senthil, A. Vishwanath, L. Balents, S. Sachdev, and M. P. A. Fisher, Deconfined quantum critical points, *Science* **303**, 1490 (2004).
- [6] S. Sachdev, Quantum magnetism and criticality, *Nat. Phys.* **4**, 173 (2008).
- [7] A. W. Sandvik, Evidence for deconfined quantum criticality in a two-dimensional Heisenberg model with four-spin interactions, *Phys. Rev. Lett.* **98**, 227202 (2007).
- [8] N. Xi, H. Chen, Z. Y. Xie, and R. Yu, Plaquette valence bond solid to antiferromagnet transition and deconfined quantum critical point of the Shastry-Sutherland model, *Phys. Rev. B* **107**, L220408 (2023).
- [9] L. Balents, Spin liquids in frustrated magnets, *Nature (London)* **464**, 199 (2010).
- [10] B. Sriram Shastry and B. Sutherland, Exact ground state of a quantum mechanical antiferromagnet, *Physica B+C* **108**, 1069 (1981).
- [11] H. Nakano and T. Sakai, Third boundary of the Shastry-Sutherland model by numerical diagonalization, *J. Phys. Soc. Jpn.* **87**, 123702 (2018).
- [12] A. Koga and N. Kawakami, Quantum phase transitions in the Shastry-Sutherland model for $\text{SrCu}_2(\text{BO}_3)_2$, *Phys. Rev. Lett.* **84**, 4461 (2000).
- [13] B. Zhao, P. Weinberg, and A. W. Sandvik, Symmetry-enhanced discontinuous phase transition in a two-dimensional quantum magnet, *Nat. Phys.* **15**, 678 (2019).

- [14] P. Corboz and F. Mila, Tensor network study of the Shastry-Sutherland model in zero magnetic field, *Phys. Rev. B* **87**, 115144 (2013).
- [15] Z. Weihong, C. J. Hamer, and J. Oitmaa, Series expansions for a Heisenberg antiferromagnetic model for $\text{SrCu}_2(\text{Bo}_3)_2$, *Phys. Rev. B* **60**, 6608 (1999).
- [16] Y. Takushima, A. Koga, and N. Kawakami, Competing spin-gap phases in a frustrated quantum spin system in two dimensions, *J. Phys. Soc. Jpn.* **70**, 1369 (2001).
- [17] M. Albrecht and F. Mila, First-order transition between magnetic order and valence bond order in a 2D frustrated Heisenberg model, *Europhys. Lett.* **34**, 145 (1996).
- [18] S. Miyahara and K. Ueda, Theory of the orthogonal dimer Heisenberg spin model for $\text{SrCu}_2(\text{Bo}_3)_2$, *J. Phys.: Condens. Matter* **15**, R327 (2003).
- [19] W. Zheng, J. Oitmaa, and C. J. Hamer, Phase diagram of the Shastry-Sutherland antiferromagnet, *Phys. Rev. B* **65**, 014408 (2001).
- [20] J. Y. Lee, Y.-Z. You, S. Sachdev, and A. Vishwanath, Signatures of a deconfined phase transition on the Shastry-Sutherland lattice: Applications to quantum critical $\text{SrCu}_2(\text{Bo}_3)_2$, *Phys. Rev. X* **9**, 041037 (2019).
- [21] A. Läuchli, S. Wessel, and M. Sigrist, Phase diagram of the quadrumerized Shastry-Sutherland model, *Phys. Rev. B* **66**, 014401 (2002).
- [22] C. Boos, S. P. G. Crone, I. A. Niesen, P. Corboz, K. P. Schmidt, and F. Mila, Competition between intermediate plaquette phases in $\text{SrCu}_2(\text{Bo}_3)_2$ under pressure, *Phys. Rev. B* **100**, 140413(R) (2019).
- [23] J. Wang, H. Li, N. Xi, Y. Gao, Q.-B. Yan, W. Li, and G. Su, Plaquette singlet transition, magnetic barocaloric effect, and spin supersolidity in the Shastry-Sutherland model, *Phys. Rev. Lett.* **131**, 116702 (2023).
- [24] J. Yang, A. W. Sandvik, and L. Wang, Quantum criticality and spin liquid phase in the Shastry-Sutherland model, *Phys. Rev. B* **105**, L060409 (2022).
- [25] L. Wang, Y. Zhang, and A. W. Sandvik, Quantum spin liquid phase in the Shastry-Sutherland model detected by an improved level spectroscopic method, *Chin. Phys. Lett.* **39**, 077502 (2022).
- [26] A. Keleş and E. Zhao, Rise and fall of plaquette order in the Shastry-Sutherland magnet revealed by pseudofermion functional renormalization group, *Phys. Rev. B* **105**, L041115 (2022).
- [27] Y. Zhou, K. Kanoda, and T.-K. Ng, Quantum spin liquid states, *Rev. Mod. Phys.* **89**, 025003 (2017).
- [28] S. Sachdev, Kagome'- and triangular-lattice Heisenberg antiferromagnets: Ordering from quantum fluctuations and quantum-disordered ground states with unconfined bosonic spinons, *Phys. Rev. B* **45**, 12377 (1992).
- [29] D. P. Arovas and A. Auerbach, Functional integral theories of low-dimensional quantum Heisenberg models, *Phys. Rev. B* **38**, 316 (1988).
- [30] N. Read and S. Sachdev, Large- N expansion for frustrated quantum antiferromagnets, *Phys. Rev. Lett.* **66**, 1773 (1991).
- [31] A. Auerbach and D. P. Arovas, Schwinger boson approaches to quantum antiferromagnetism, in *Introduction to Frustrated Magnetism*, Springer Series in Solid State Sciences, edited by C. Lacroix, P. Mendels, and F. Mila (Springer, Berlin, 2011), Chap. 14, pp. 365–378.
- [32] X.-G. Wen, Quantum orders and symmetric spin liquids, *Phys. Rev. B* **65**, 165113 (2002).
- [33] F. Wang and A. Vishwanath, Spin-liquid states on the triangular and kagomé lattices: A projective-symmetry-group analysis of Schwinger boson states, *Phys. Rev. B* **74**, 174423 (2006).
- [34] C. Tchernyshyov, R. Moessner, and S. L. Sondhi, Flux expulsion and greedy bosons: Frustrated magnets at large N , *Europhys. Lett.* **73**, 278 (2006).
- [35] A. Polyakov, Quark confinement and topology of gauge theories, *Nucl. Phys. B* **120**, 429 (1977).
- [36] X. Yang and F. Wang, Schwinger boson spin-liquid states on square lattice, *Phys. Rev. B* **94**, 035160 (2016).
- [37] J. Takano, H. Tsunetsugu, and M. E. Zhitomirsky, Self-consistent spin wave analysis of the magnetization plateau in triangular antiferromagnet, *J. Phys.: Conf. Ser.* **320**, 012011 (2011).
- [38] V. V. Mkhitarian and L. Ke, Self-consistently renormalized spin-wave theory of layered ferromagnets on the honeycomb lattice, *Phys. Rev. B* **104**, 064435 (2021).
- [39] H. Nakano and T. Sakai, Large-scale numerical-diagonalization study of the Shastry-Sutherland model, *JPS Conf. Proc.* **38**, 011166 (2023).
- [40] R. Moessner, S. L. Sondhi, and E. Fradkin, Short-ranged resonating valence bond physics, quantum dimer models, and Ising gauge theories, *Phys. Rev. B* **65**, 024504 (2001).
- [41] R. Boyack, C.-H. Lin, N. Zerf, A. Rayyan, and J. Maciejko, Transition between algebraic and \mathbb{Z}_2 quantum spin liquids at large N , *Phys. Rev. B* **98**, 035137 (2018).
- [42] A. M. Essin and M. Hermele, Classifying fractionalization: Symmetry classification of gapped \mathbb{Z}_2 spin liquids in two dimensions, *Phys. Rev. B* **87**, 104406 (2013).
- [43] T. Holstein and H. Primakoff, Field dependence of the intrinsic domain magnetization of a ferromagnet, *Phys. Rev.* **58**, 1098 (1940).
- [44] S. Sachdev, Quantum phase transitions of antiferromagnets and the cuprate superconductors, in *Modern Theories of Many-Particle Systems in Condensed Matter Physics*, edited by D. C. Cabra, A. Honecker, and P. Pujol (Springer, Berlin, 2012), pp. 1–51.